



ESCUELA TÉCNICA SUPERIOR DE INGENIERÍA  
(ICAI)

GRADO EN INGENIERÍA ELECTROMECÁNICA

Especialidad Mecánica

# **Design of a Battery Cooling System for the Illini Formula Electric Vehicle**

Author: Alberto Freire Montero

Director: Prof. Anthony Jacobi

Madrid

2017-2018



## **AUTHORIZATION FOR DIGITALIZATION, STORAGE AND DISSEMINATION IN THE NETWORK OF END-OF-DEGREE PROJECTS, MASTER PROJECTS, DISSERTATIONS OR BACHILLERATO REPORTS**

### ***1. Declaration of authorship and accreditation thereof.***

The author Mr. /Ms. ALBERTO FREIRE MONTERO

**HEREBY DECLARES** that he/she owns the intellectual property rights regarding the piece of work: DESIGN OF A BATTERY COOLING SYSTEM FOR THE ILLINI FORMULA ELECTRIC VEHICLE that this is an original piece of work, and that he/she holds the status of author, in the sense granted by the Intellectual Property Law.

### ***2. Subject matter and purpose of this assignment.***

With the aim of disseminating the aforementioned piece of work as widely as possible using the University's Institutional Repository the author hereby **GRANTS** Comillas Pontifical University, on a royalty-free and non-exclusive basis, for the maximum legal term and with universal scope, the digitization, archiving, reproduction, distribution and public communication rights, including the right to make it electronically available, as described in the Intellectual Property Law. Transformation rights are assigned solely for the purposes described in a) of the following section.

### ***3. Transfer and access terms***

Without prejudice to the ownership of the work, which remains with its author, the transfer of rights covered by this license enables:

- a) Transform it in order to adapt it to any technology suitable for sharing it online, as well as including metadata to register the piece of work and include "watermarks" or any other security or protection system.
- b) Reproduce it in any digital medium in order to be included on an electronic database, including the right to reproduce and store the work on servers for the purposes of guaranteeing its security, maintaining it and preserving its format.
- c) Communicate it, by default, by means of an institutional open archive, which has open and cost-free online access.
- d) Any other way of access (restricted, embargoed, closed) shall be explicitly requested and requires that good cause be demonstrated.
- e) Assign these pieces of work a Creative Commons license by default.
- f) Assign these pieces of work a HANDLE (*persistent URL*). by default.

### ***4. Copyright.***

The author, as the owner of a piece of work, has the right to:

- a) Have his/her name clearly identified by the University as the author
- b) Communicate and publish the work in the version assigned and in other subsequent versions using any medium.
- c) Request that the work be withdrawn from the repository for just cause.
- d) Receive reliable communication of any claims third parties may make in relation to the work and, in particular, any claims relating to its intellectual property rights.

### ***5. Duties of the author.***

The author agrees to:

- a) Guarantee that the commitment undertaken by means of this official document does not infringe any third party rights, regardless of whether they relate to industrial or intellectual property or any other type.

- b) Guarantee that the content of the work does not infringe any third party honor, privacy or image rights.
- c) Take responsibility for all claims and liability, including compensation for any damages, which may be brought against the University by third parties who believe that their rights and interests have been infringed by the assignment.
- d) Take responsibility in the event that the institutions are found guilty of a rights infringement regarding the work subject to assignment.

**6. Institutional Repository purposes and functioning.**

The work shall be made available to the users so that they may use it in a fair and respectful way with regards to the copyright, according to the allowances given in the relevant legislation, and for study or research purposes, or any other legal use. With this aim in mind, the University undertakes the following duties and reserves the following powers:

- a) The University shall inform the archive users of the permitted uses; however, it shall not guarantee or take any responsibility for any other subsequent ways the work may be used by users, which are non-compliant with the legislation in force. Any subsequent use, beyond private copying, shall require the source to be cited and authorship to be recognized, as well as the guarantee not to use it to gain commercial profit or carry out any derivative works.
- b) The University shall not review the content of the works, which shall at all times fall under the exclusive responsibility of the author and it shall not be obligated to take part in lawsuits on behalf of the author in the event of any infringement of intellectual property rights deriving from storing and archiving the works. The author hereby waives any claim against the University due to any way the users may use the works that is not in keeping with the legislation in force.
- c) The University shall adopt the necessary measures to safeguard the work in the future.
- d) The University reserves the right to withdraw the work, after notifying the author, in sufficiently justified cases, or in the event of third party claims.

Madrid, on 20..... of JUNE 2018.....

**HEREBY ACCEPTS**

Signed.....

Reasons for requesting the restricted, closed or embargoed access to the work in the Institution's Repository

Declaro, bajo mi responsabilidad, que el Proyecto presentado con el título  
...Design of a Battery Cooling System...  
for the Illini Formula Electric Vehicle...  
en la ETS de Ingeniería - ICAI de la Universidad Pontificia Comillas en el  
curso académico ..2017/2018. es de mi autoría, original e inédito y  
no ha sido presentado con anterioridad a otros efectos. El Proyecto no es  
plagio de otro, ni total ni parcialmente y la información que ha sido tomada  
de otros documentos está debidamente referenciada.

  
Alberto Freire Montero  
Fdo.: (Nombre del alumno) Fecha: 08 / 05 / 18.



Autorizada la entrega del proyecto  
EL DIRECTOR DEL PROYECTO

ANTHONY M. JACOBI  
Fdo.: (Nombre del Director) Fecha: 07 / 05 / 18.



# **DISEÑO DE UN SISTEMA DE REFRIGERACIÓN PARA EL VEHÍCULO DE ILLINI FORMULA ELECTRIC**

**Autor: Freire Montero, Alberto**

Director: Jacobi, Anthony

Entidad Colaboradora: ICAI - Universidad Pontificia Comillas, University of Illinois at Urbana-Champaign

## **RESUMEN DEL PROYECTO**

Illini Formula Electric (IFE) es un equipo de competición patrocinado por la University of Illinois at Urbana-Champaign, que compite anualmente en la Formula SAE (FSAE), en la categoría eléctrica (EV). Esta competición brinda la oportunidad a diferentes estudiantes de grado y postgrado de diseñar un monoplaza eléctrico y competir contra otros equipos de todas partes del mundo.

Estos vehículos son impulsados por un motor eléctrico que funciona con un acumulador. Este acumulador consiste en un paquete de baterías de iones de litio. IFE actualmente fabrica su propio acumulador con celdas caseras. A partir del próximo año y en adelante, implementarán módulos de baterías Samsung Li8P25RT disponibles en el mercado. Estos módulos tienen una mayor densidad de energía y se espera que suministren más potencia al motor. Sin embargo, al pasar mayor corriente a través del acumulador, se generará una cantidad excesiva de calor. Este exceso de calor puede conducir a una disminución de la salida de corriente y a la degradación del paquete de iones de litio, por lo que se requiere un sistema de refrigeración para transferir eficazmente el calor a un medio externo. El objetivo de este proyecto es diseñar un sistema de refrigeración que facilite el rechazo de calor desde el acumulador, aumentando la capacidad de extracción de energía, y así contribuir a un mejor rendimiento del vehículo.

## **Especificaciones de diseño**

Aunque la competición permite gran libertad de diseño al tener reglas poco estrictas, existen algunas normas relacionadas con la seguridad y buenas prácticas de

ingeniería. No hay regulaciones con respecto al diseño del sistema de refrigeración del acumulador. Sin embargo, el acumulador debe colocarse en una carcasa que siga las reglas dadas por FSAE, por lo que el sistema de refrigeración no debe interferir con ellas. Estas reglas están relacionadas especialmente con medidas de seguridad, tales como resistencia al impacto, resistencia al agua y resistencia al fuego, por ejemplo.

## **Análisis de fuentes de calor**

Después de analizar las diferentes fuentes de calor posibles, que consistían en acumulador, motor eléctrico y asfalto, se concluye que el acumulador era la única fuente de calor relevante en este estudio, ya que el motor eléctrico ya tiene su propio sistema de refrigeración, mientras que el calor transferido por la radiación del asfalto se consideró insignificante.

Los módulos de baterías comerciales se eligen para suministrar una corriente más alta, y esto requiere un sistema de refrigeración eficiente, basado en una predicción teórica de generación de calor y posterior experimentación para la verificación. Los cálculos teóricos muestran que el calor que se espera de la batería es la combinación de pérdida de energía eléctrica debida a la resistencia interna y la emisión de calor de las reacciones químicas, llegando hasta 13kW.

## **Soluciones propuestas**

Se propusieron diferentes soluciones para afrontar problema. Estas soluciones incluían tanto soluciones de refrigeración líquida como refrigeración por aire, todas ellas provistas por el patrocinador Novark Technologies.

Se ha decidido excluir la posibilidad de tener un sistema de refrigeración líquida. Esto fue solicitado específicamente por el IFE debido a las restricciones de la bomba de agua existente en el vehículo eléctrico. En su lugar, se ha elegido un sistema que combina la conducción y la convección directa con el aire, que consta de disipadores de calor, tubos de calor y aletas planas.

## **Análisis y Experimentos**

Se completó análisis del sistema de refrigeración con una especificación geométrica detallada para los componentes del sistema y un análisis de costes. La transferencia de calor y la caída de presión esperada en el diseño se calcularon mediante

el uso de modelos de análisis de elementos finitos (FEA) y simulaciones de dinámica de fluidos computacional (CFD).

Los resultados de simulación para la caída de presión se compararon con los experimentos del túnel de viento realizados. También se llevó a cabo un experimento para verificar el modelo de generación de calor del acumulador, que confirmó el análisis FEA.

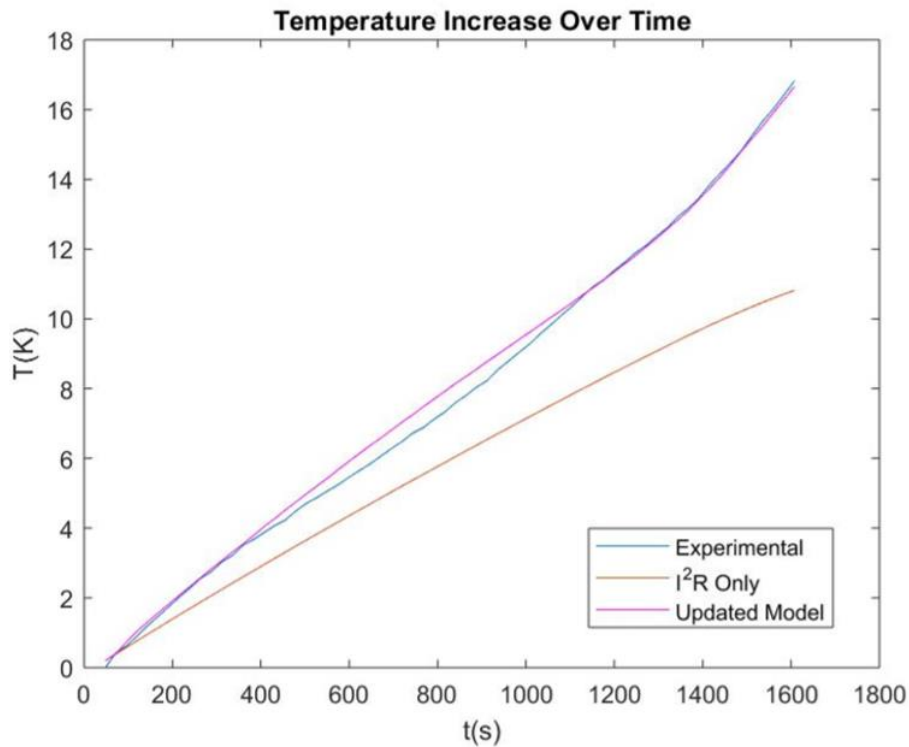


Figure 1

## Diseño final

Como se mencionó anteriormente, el sistema de enfriamiento consistirá en disipadores de calor, tubos de calor, aletas y ventiladores, todo dentro de una carcasa.

Los disipadores de calor se fabricarán con aluminio 6061 y están diseñados para ajustarse a la geometría de los paquetes de baterías. La termopasta se aplicaría entre los disipadores y las baterías de manera que haya la mayor superficie en contacto mientras se reduce la resistencia térmica.

Los tubos de calor se insertarán en los disipadores de calor en los orificios diseñados con ese fin. El calor irá desde el extremo caliente del tubo de calor hasta el extremo frío, donde las aletas serán soldadas.

Las aletas rechazarán el calor con el aire, que será soplado por 6 ventiladores elegidos específicamente para cumplir con nuestros requisitos, EBM-PAPST 4118 N / 2H8P.

Todos estos elementos de nuestro sistema de refrigeración se colocarán dentro de una carcasa de acumulador diseñada en función de la caída de presión que pretendemos, que IFE fabricará una vez que hayan llegado todos los módulos de la batería.

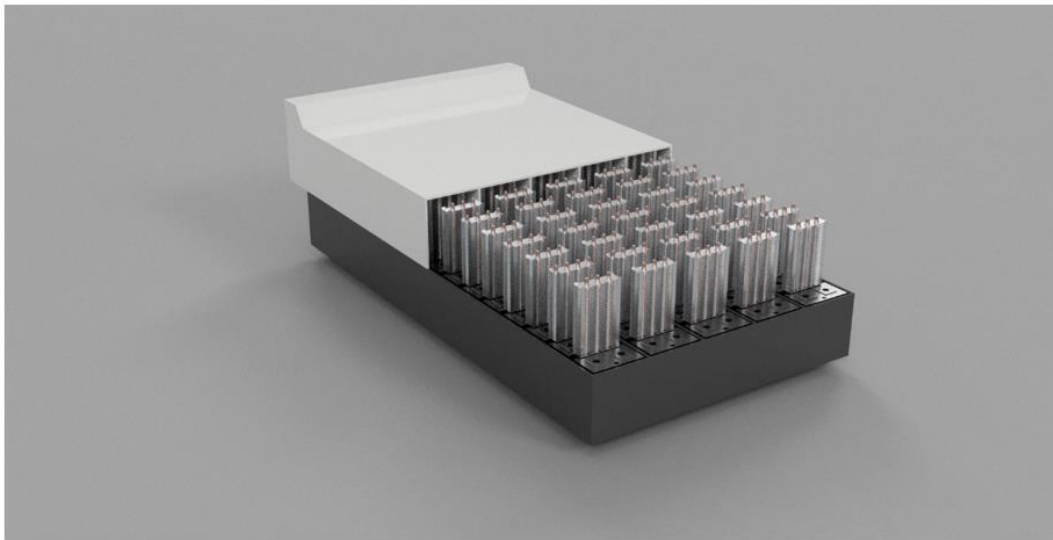


*Figure 2*

## **Conclusiones**

Con el diseño completo, la fabricación del prototipo está patrocinada por Novark Technologies, sin costo para el equipo. El presupuesto gastado es de 1132\$ para todos los experimentos y compras requeridas.

El sistema de refrigeración se implementará completamente en el vehículo que participa en la competición de 2019. Los proyectos futuros deberán probar el diseño en colaboración con IFE una vez que el vehículo esté completamente operativo. Más datos experimentales permitirán mejoras y modificaciones al prototipo

# **DESIGN OF A BATTERY COOLING SYSTEM FOR THE ILLINI FORMULA ELECTRIC VEHICLE**

**Author: Freire Montero, Alberto**

Director: Jacobi, Anthony

Collaborating Entity: ICAI - Universidad Pontificia Comillas, University of Illinois at Urbana-Champaign

## **PROJECT ABSTRACT**

Illini Formula Electric (IFE) is an electric vehicle (EV) competition team sponsored at the University of Illinois at Urbana-Champaign which races annually at the Formula SAE (FSAE) competition. This competition brings the opportunity to different undergraduate and graduate students to design a single-seater electric vehicle and compete against other teams from other parts of the world.

These vehicles are driven by an electric motor, which is powered by an accumulator. This accumulator consists of a group of Lithium-ion battery modules. IFE currently fabricates their own accumulator with homemade Li-ion cells. From next year and on, they will be implementing commercially available Samsung Li8P25RT battery modules. These modules have a higher energy density and are expected to supply more power to the motor. However, when large amounts current pass through the accumulator an excess amount of waste heat will be generated. This excess waste heat can lead to lowered current output and due to degradation of the lithium ion pack, so a cooling system is required to effectively transfer the waste heat to an external sink. Our goal is to design a cooling system to facilitate heat rejection from the accumulator, increasing power draw capability, and thus contribute to better vehicle performance.

## **Design Specifications**

Although the competition allows freedom of design by having very relaxed regulations, there exist some regulations related to safety and good engineering practices. There are no regulations regarding the cooling design of the accumulator. However, the accumulator should be placed in a housing which follows the rules given by FSAE, so the

cooling system must not interfere with them. These rules are related specially to safety measures, such impact resistance, water resistance and fire resistance, for example.

## **Heat Sources Analysis**

After analyzing the different possible heat sources, which consisted of accumulator, drive motor and the asphalt, we concluded that the accumulator was the only heat source relevant in our study, as the drive motor already had its own cooling system, while the heat transferred by radiation from the asphalt was considered negligible.

The commercial battery modules are chosen to supply a higher current, and this would require an efficient cooling system based on our theoretical prediction of the waste heat generation and battery experiment for verification. Theoretical calculations show the waste heat expected from the battery is the combination of electrical power loss due to internal resistance and heat conversion from chemical reactions and rises up to 13kW.

## **Proposed Solutions**

Different solutions were proposed to overcome the problem. These solutions included both liquid-cooling and air-cooling solutions, all of them provided by our sponsor Novark Technologies

We have decided to exclude the possibility of having a liquid cooling system. This was specifically requested by the IFE due to power and heat capacity restrictions of the existing liquid pump system on the electric vehicle. Instead, we chose a system that combines conduction and direct air convection, consisting of heat sinks, heat pipes and plate fins.

## **Analysis and Experiments**

An analysis led design of the cooling system was completed with a detailed geometrical specification for the system components and cost analysis. The heat transfer and expected pressure drop from our mechanism was calculated using thermal finite element analysis (FEA) modeling and computational fluid dynamics (CFD) simulations.

The simulation results for pressure drop were compared to the wind tunnel experiments we conducted. An experiment to verify the waste heat model of the accumulator was also ran, confirming our FEA analysis.

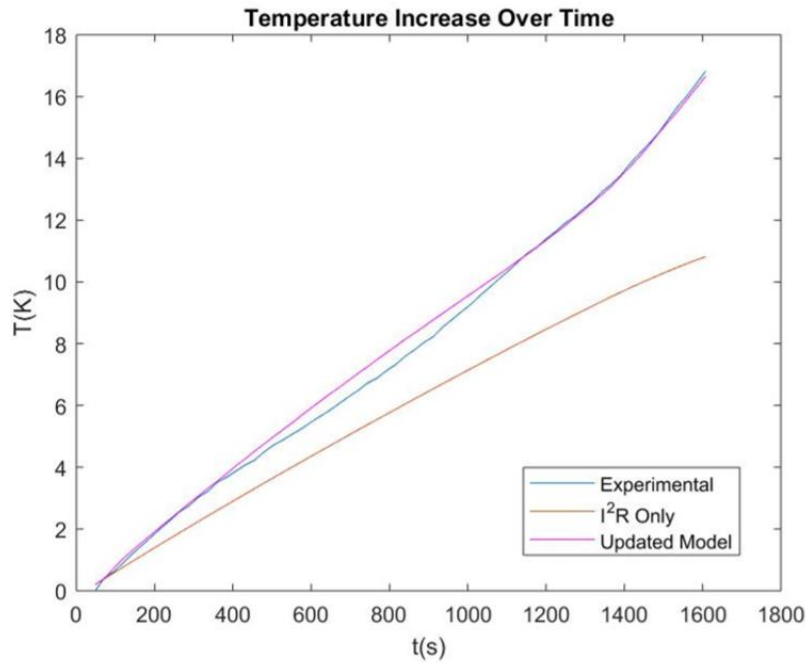


Figure 1

## Final Design

As mentioned before, the cooling system will consist of heat sinks, heat pipes, fins and fans, all inside an accumulator box.

The heat sinks will be manufactured with Aluminum 6061 and are designed to fit the geometry of the battery packs. Thermopaste would be applied in between so there is the most surface in contact while reducing the thermal resistance.

Heat pipes will be inserted in the heat sinks in the holes designed with that purpose. Heat will travel from the hot end of the heat pipe to the cold end, where the fins will be soldered.

Fins will reject the heat to the ambient air, which will be blown by 6 fans specifically chosen to meet our requirements, EBM-PAPST 4118 N/2H8P.

All these elements of our cooling system will be place inside an accumulator housing designed based on the pressure drop we are aiming for, which IFE will manufacture once all the battery modules have arrived.

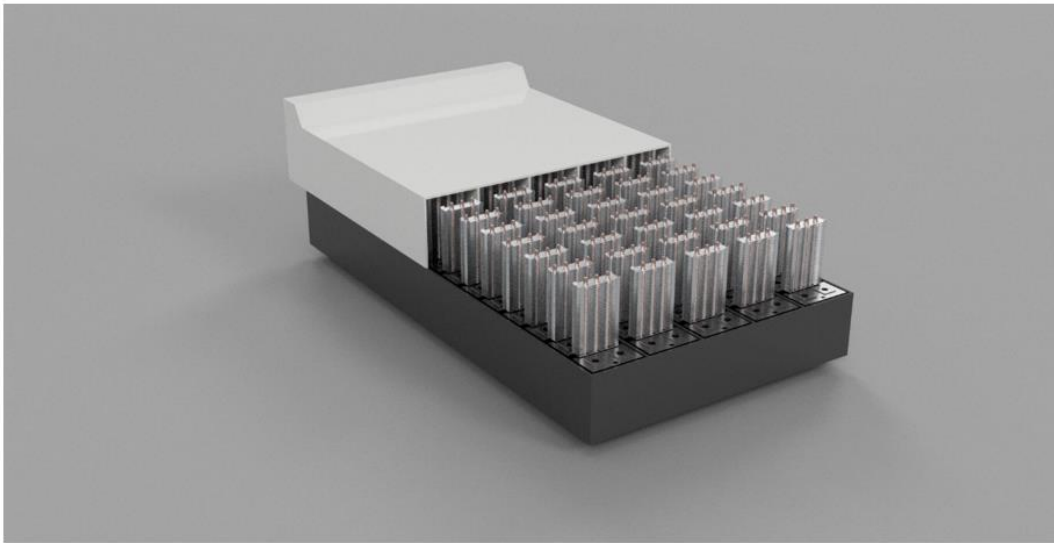


*Figure 2*

## **Conclusions**

With the design complete, the prototype manufacture is sponsored by Novark Technologies, at no cost to the team. Our budget spent is \$1132 for the whole experiments and purchases required.

Our cooling system will be fully implemented in the vehicle that participates in the 2019 competition. Future projects shall test the design in collaboration with IFE once the vehicle is fully operative. Further experimental data will allow for improvements and modifications to the prototype.





## **Acknowledgements**

To my parents, for giving me the opportunity to study where I wanted, what I wanted, supporting me all the time.

To my friends, which have made this four years in Madrid and Champaign the best years of my life.

To ICAI, providing me one of the best educations you could ask for, and for letting me experience other type of culture studying abroad. To the professors, their dedication and effort.

To UIUC Mechanical Department, for letting me take part of Senior Design Project. Thank you to Prof. Anthony Jacobi, for guiding me through this project. Thank you to my fellow partners, David, Phil, Le and Yeonsoo, which helped me thorough the whole semester.



# CONTENTS

1.	INTRODUCTION .....	7
1.1.	Problem Statement .....	7
1.2.	Project Objective.....	8
1.3.	Design Specifications .....	8
2.	PRIOR ART .....	9
2.1.	Basic Concepts of Heat Transfer .....	9
2.1.1.	Conduction .....	10
2.1.2.	Convection .....	11
2.1.3.	Radiation .....	13
2.2.	Need of a Cooling System .....	14
2.3.	Air-Cooling Systems.....	14
2.3.1.	Fins and Extended Surfaces .....	15
2.4.	Liquid-Cooling Systems .....	19
2.4.1.	Functioning of a Liquid-Cooling System.....	20
2.4.2.	Water Pump.....	20
2.4.3.	Cooling Fluid.....	21
2.4.4.	Thermostat.....	21
2.4.5.	Radiator .....	22
3.	HEAT SOURCES AND ASSUMPTIONS .....	23
3.1.	Overview.....	23
3.2.	Accumulator.....	23
3.3.	Motor .....	27
3.4.	Track .....	27
4.	PROPOSED CONCEPTS .....	29
4.1.	Brainstorming .....	29
4.2.	Fins and Heat Pipes.....	29
4.3.	Vapor Chambers .....	30
4.4.	Vacuum Brazed Cold Plates .....	31
4.5.	Loop Heat Pipes.....	32
4.6.	Complementary Concepts.....	33
5.	CONCEPT DEVELOPMENT AND INITIAL DESIGN .....	35
6.	ANALYSIS .....	37

6.1.	FEA Simulations.....	37
6.2.	Air-side Heat Transfer .....	40
6.3.	CFD Simulations.....	43
7.	EXPERIMENTS.....	47
7.1.	Battery Module Waste Heat Generation Experiment .....	47
7.2.	Pressure Drop Experiment of Four Fin Arrays .....	51
8.	FINAL DESIGN.....	55
8.1.	Heat Sinks .....	55
8.2.	Heat Pipes .....	55
8.3.	Fins.....	56
8.4.	Fans.....	58
8.5.	Accumulator Case.....	60
8.6.	Phase-Change Materials .....	61
9.	FUTURE EXPERIMENTS .....	63
10.	PROJECT DELIVERABLES AND BUDGET.....	65
11.	CONCLUSIONS .....	67
12.	REFERENCES .....	69
13.	APPENDIX A: OLD ACCUMULATOR .....	71
14.	APPENDIX B: CAD DESIGN.....	75
15.	APPENDIX C: WIND TUNNEL SETUP.....	79
16.	APPENDIX D: VOLTAGE EXPERIMENT .....	85
17.	APPENDIX E: FIN ANALYSIS MATLAB CODE.....	91
18.	APPENDIX F: BATTERY DATA SHEET .....	93

# LIST OF FIGURES

Figure 1: Example of Conduction .....	11
Figure 2: Natural and Forced Convection .....	12
Figure 3: Example of Air-Cooled System .....	15
Figure 4: Types of Fins.....	16
Figure 5; Different Fin Arrays.....	16
Figure 6: Fin Parameters .....	17
Figure 7: Example of Liquid-Cooled System.....	19
Figure 8: Water Pump .....	20
Figure 9: Thermostat .....	21
Figure 10: Radiator.....	22
Figure 11: Initial Waste Heat Model .....	24
Figure 12: Updated Waste Heat Model .....	25
Figure 13: IFE Duty Cycle .....	26
Figure 14: Drive Motor .....	27
Figure 15: Fins and Heat Pipes.....	30
Figure 16: Vapor Chambers .....	31
Figure 17: Vacuum Brazed Cold Plates .....	32
Figure 18: Loop Heat Pipe.....	33
Figure 19: Interface Simulation.....	37
Figure 20: Interface Simulation, Battery Side .....	38
Figure 21: Interface Simulation, Heat Sink Side .....	38
Figure 22: Temperature Profile .....	39
Figure 23: Heat Transfer Rate vs Fin Length .....	41
Figure 24: Steady State Pressure Drop Simulation .....	44
Figure 25: 10 s Pressure Drop Simulation.....	45
Figure 26: Battery Module .....	47
Figure 27: Sensors Circuit Diagram .....	48
Figure 28: Experiment Setup.....	49
Figure 29: IR Camera Picture.....	49
Figure 30: Sensors and Surface Temperature.....	50
Figure 31: Surface Temperature for Different Batteries .....	51
Figure 32: Pressure Drop Experiment Setup .....	52

Figure 33: Heat Sink.....	55
Figure 34: Heat Pipe.....	56
Figure 36: Fin Design.....	57
Figure 35: Sample of Heat Sinks, Heat Pipes and Fins.....	57
Figure 37: Fan Specs.....	58
Figure 38: Fan Technical Description.....	58
Figure 39: Fan Operation Curve.....	59
Figure 40: Typical Behavior of Two Fans in Series.....	60
Figure 41: Final Design Configuration.....	60
Figure 42: Final Design Half Cut.....	61
Figure 43: Final Design without Case.....	63

# LIST OF TABLES

Table 1: FSAE Regulations .....	8
Table 2: Specific Heats.....	9
Table 3: Thermal Conductivities .....	10
Table 4: Coefficient of Convection .....	13
Table 5: Emisivities .....	14
Table 6: Battery Data Sheet.....	23
Table 7: Heat Transfer Rate vs Fin Spacing and Fin Thickness .....	42
Table 8: Budget Spent .....	65



# 1. INTRODUCTION

## 1.1. Problem Statement

Formula SAE organizes an annual competition in which college students from around the world will compete with their own single-seater vehicle. In 2010, the organization introduced the subcategory competition involving solely electrically powered vehicles.

The competition consists of four main events: acceleration, skid pad, auto-cross, and endurance. The acceleration event evaluates the vehicle's ability to accelerate down a straight line in flat pavement, typically lasting less than ten seconds. The skid pad event, lasting for about five minutes, evaluates the vehicle's handling by observing how well it can corner on a flat surface while making a constant-radius turn. The auto-cross event evaluates maneuverability by timing the vehicle for a single lap without other competitors on the same track. The endurance event evaluates the power efficiency of the vehicle, by having the vehicle run on track until the accumulator is completely drained of power, or a component/system failure occurs.

Since, the skid pad and auto-cross events are designed to test the mechanical capabilities of the vehicle, our cooling design and analysis are based on situations that are relevant to the acceleration and endurance events.

To boost the power output of the vehicle, IFE is designing a new accumulator with higher energy density and a higher current output compared to its existing homemade accumulator, consisted of a total of 600 Samsung INR 18650-25R battery cells, modulized by 8. This implies that the new accumulator will have a higher waste heat generation rate, as well as higher power output. If waste heat remains inside the accumulator without being rejected into ambient air, its temperature will rise, resulting in faster battery degradation and lower battery efficiency.

## 1.2. Project Objective

The primary objective of this project is to design a cooling system to keep the temperature of the accumulator below the target temperature of 45 °C. The data sheet for the Samsung 18650 25R battery suggests the maximum operating temperature is 60 °C for discharging and 45 °C for charging. Since the accumulator will undergo both discharging and charging cycles during the competition, we chose 45 °C to be our target temperature.

The vehicle that utilizes our solution must also comply with competition regulations enforced by Formula SAE. Furthermore, the installation of the cooling system must result in an overall increase in energy efficiency of the vehicle.

## 1.3. Design Specifications

The cooling system must comply with all FSAE competition regulations in addition to achieving the performance standards above. Relevant clauses of the rules are manifested in terms of design specifications in Table 1.

<b>Constraint</b>	<b>Detail</b>
Dimensions	600 x 700 x 200 mm
Removability	Accumulator is charged outside the vehicle
Waterproof	No leakage after spraying water for 2 minutes
Fireproof	UL94 V-0
Crash Resistance	Horizontal: 40 g Vertical: 20 g
Insulation	Electrical insulation

*Table 1: FSAE Regulations*

## 2. PRIOR ART

### 2.1. Basic Concepts of Heat Transfer

We define heat as the energy transmitted from one closed system to another closed system or to its surroundings when there is a difference in temperature between them. Usually represented with the letter  $Q$ , heat transfers from the hot to the cold body pretending to balance the temperature of both.

The expression which relates the heat exchanged by a system is the one that follows:

$$Q = mC\Delta T$$

*Equation 1*

Where  $m$  is the mass of the system,  $C$  is the specific heat of it and  $\Delta T$  is the change in temperature that it suffers. Specific heat is a property of each material, and it corresponds to the energy necessary to increase 1 kg of it by 1 K. Here is a table with the specific heat for different elements.

Substance	Specific Heat (J/kg°C)
Copper	387
Gold	129
Iron	448
Silver	234
Glass	837
Wood	1700
Ice (-5 °C)	2090
Water (15 °C)	4186
Steam (100 °C)	2010
Sand	830
Alcohol	2300

*Table 2: Specific Heats*

It is clear that there will be situations along this project in which it will be heat transfer from one system to another, as there is a difference in temperature between the

components of the cooling system. For example, between the heat sinks and the heat pipes by conduction and between the fins and the air by forced convection.

There are three main ways of transferring heat: conduction, convection and radiation. In this study we will focus especially on the first two, as radiation is almost negligible in our design.

### 2.1.1. Conduction

Conduction is the phenomenon that occurs between two or more systems in contact with different temperature, transferring heat from the hot to the cold system. It also occurs between points in the same system with different temperatures. Although it is typical in solid systems, it can appear in fluids which are stationary.

Heat transfer by conduction happens due to the vibrating energy of the system and, in metals, due to the free flux of electrons.

The equation which rules conduction is Fourier's Law, obtained experimentally:

$$q = -Ak\nabla T$$

*Equation 2*

Where  $A$  is the heat transfer area,  $k$  is the conductivity, measured in  $\frac{W}{mK}$  and  $\nabla T$  is the gradient in temperature. The - sign indicates that the flux travels in the direction of the decreasing temperatures. Some typical conductivity values are:

Substance	Thermal Conductivity (W/mK)
Copper	399
Gold	317
Aluminum	237
Iron	80.2
Stainless Steel	15.1
Glass	0.81
Water	0.6
Air	0.026

*Table 3: Thermal Conductivities*

In this table we can appreciate the great conductivity values metals have, as a result of the free flux of electrons mentioned before. It is also remarkable the low values obtained from liquids and gases. Energy is transmitted by the exchange in momentum between molecules, a transfer mechanism not as effective as the one present in metals. This is the main reason because fluids and gases have lower conductivity values than metals.

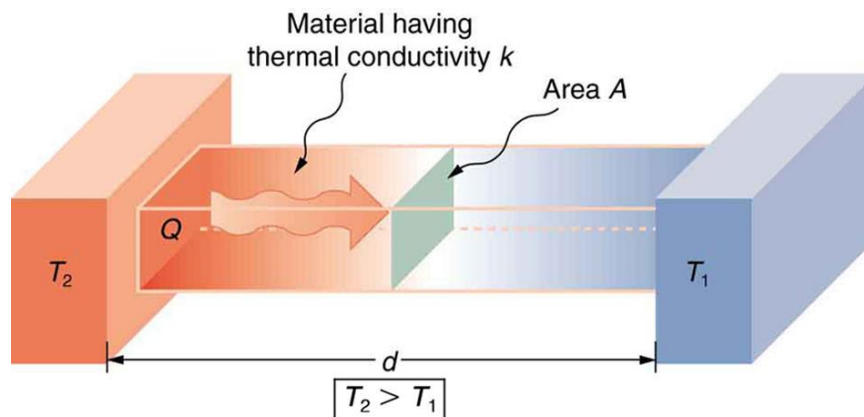
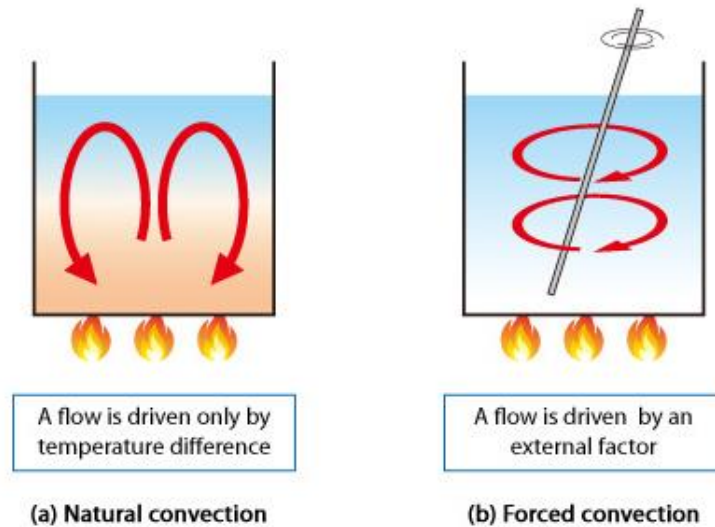


Figure 1: Example of Conduction

In our system, conduction will happen between the accumulator and the heat sinks, heat sinks and heat pipes, and heat pipes and fins.

### 2.1.2. Convection

Convection is the heat transfer that occurs between a body or surface in contact with a fluid, gas or liquid. It is composed by conduction between the fluid molecules and advection, the movement of the fluid. There are two types of convection: natural and forced. In natural convection there is no interference in the system, making the renovation of the fluid slower, hence making the heat transfer lower as well. In forced convection, mechanical elements such as fans or pumps are used to move the fluid, increasing the heat transfer in the process.



*Figure 2: Natural and Forced Convection*

Convection is ruled by Newton's Law of Cooling:

$$q = hA(T_{\infty} - T_s)$$

*Equation 2*

Where  $A$  is the heat transfer area,  $T_{\infty}$  the temperature of free flow of the fluid,  $T_s$  the temperature of the surface and  $h$  the coefficient of convection, a parameter obtained experimentally, measured in  $\frac{W}{m^2 K}$ . The coefficient of convection shows the thermal power transmitted between the surface and the fluid when the difference in temperature is 1 K. It depends of the properties of the fluid, the geometry of the surface and the configuration of the fluid surrounding the surface.  $h$  is also very related to the thermal conductivity of the fluid, as in the contact region with the surface there is no relative speed between them two, making all the heat transfer rely on conduction.

Some typical values of coefficient of convection  $h$  are:

<b>Fluid</b>	<b>Convective Coefficient <math>h</math> (W/m<sup>2</sup>K)</b>
Air	6 - 30
Air (Forced Convection)	30 - 300
Water	20 - 100
Water (Forced Convection)	300 - 18000
Water (Boiling)	3000 - 60000
Oil (Forced Convection)	60 - 1800
Refrigerants (Boiling)	500 - 3000
Refrigerants (Condensing)	1500 - 5000
Steam (Condensing)	6000 - 120000

*Table 4: Coefficient of Convection*

Convection will be relevant in our system as it is the way we are transferring heat from the fins to the ambient air, helping reduce the temperature of the whole accumulator.

### **2.1.3. Radiation**

As radiation is almost negligible in our design, a rough explanation of how it transfers heat will be given.

Radiation transfers heat through electromagnetic waves, emitted by matter above the absolute zero, 0 K. It is ruled by the Stefan-Boltzmann Law, which states that the power transmitted through radiation corresponds to:

$$q = \varepsilon \sigma A T_s^4$$

*Equation 3*

Where  $A$  is the surface of the system,  $T_s$  is the temperature of the surface,  $\sigma$  is the Stefan-Boltzmann constant and  $\varepsilon$  is the thermal emissivity, which varies from 0 to 1, and depends of the material of the body. Some typical values of radiation are:

<b>Material</b>	<b>Emissivity</b>
Polished Aluminum	0.07
Polish Gold	0.03

Black Paint	0.98
Water	0.96
Asphalt	0.85-0.93
Wood	0.82-0.92
Stainless Steel	0.17
Vegetation	0.92-0.96
Human Skin	0.95

*Table 5: Emisivities*

## **2.2. Need of a Cooling System**

Since the early beginnings of the automobile and up to this date, all the combustion engines dispose of a cooling system which rejects the excess of heat waste generated by the engine and guarantees the optimal temperature for it and its components to operate.

With the recent appearance of the electric vehicle this has not changed at all, since although there is no combustion engine to refrigerate, there are other components which are necessary to refrigerate as well, such as the electric motor or the accumulator, which is our case.

The current flow in the batteries of electric cars produces their cells to heat up. The greater current flux, the greater the heating. The performance of lithium-ion batteries depends to a large extent on their operating temperature: they suffer the Goldilocks effect, they do not work well when subjected to too cold or too hot.

Exposing them to temperatures that are too low or too high can cause permanent damage to the batteries and accelerated degradation. Therefore, a temperature control system is necessary for the batteries, which cool or heat them when necessary.

Historically, there are two main ways to refrigerate the components of the powertrain of a vehicle, using an air-cooled system or a liquid-cooled system.

## **2.3. Air-Cooling Systems**

Air cooling is commonly used in motorcycles and applications in which low power is required. The excess in heat is transmitted to the air by convection. To increase this convection, fins are used to expand the area in contact with the air, boosting the power

transfer in between the component and the air. Sometimes, fans are introduced to enhance forced convection.

The main advantage of this kind of refrigeration is its simplicity, as there are no moving components or ducts in which can appear wear or leakage. This simplicity also translates into some other advantages, as lightweight, cheap cost and no maintenance required. However, air-cooled systems have their downsides. The refrigeration is unstable, as it depends a lot on the speed the vehicle is travelling; there exist the possibility of overheating in very hot scenarios, as the power they can reject is much lower than the liquid-cooled systems. Finally, these systems are less efficient, as there are required huge



*Figure 3: Example of Air-Cooled System*

amounts of air to obtain a similar result as if we were cooling the component with a liquid system.

### **2.3.1. Fins and Extended Surfaces**

As mentioned in the previous section, fins are the main component in an air-cooled system, and are used to transfer heat through conduction, along themselves, and convection, in contact with the air.

The main objective of the fins is to extend the area in contact with the air, so we can increase the power transfer from our system to the air. In a similar way, we can obtain the same power transfer with a smaller variation in temperature, preventing some components to fail.

There are different types of fins and can be classified based on its geometry. Plain fins are those which its base is a plain. Annular fins are those which base is a cylindrical surface. Finally, needle fins are those which have a long cylindrical shape, being it base a plain, too.

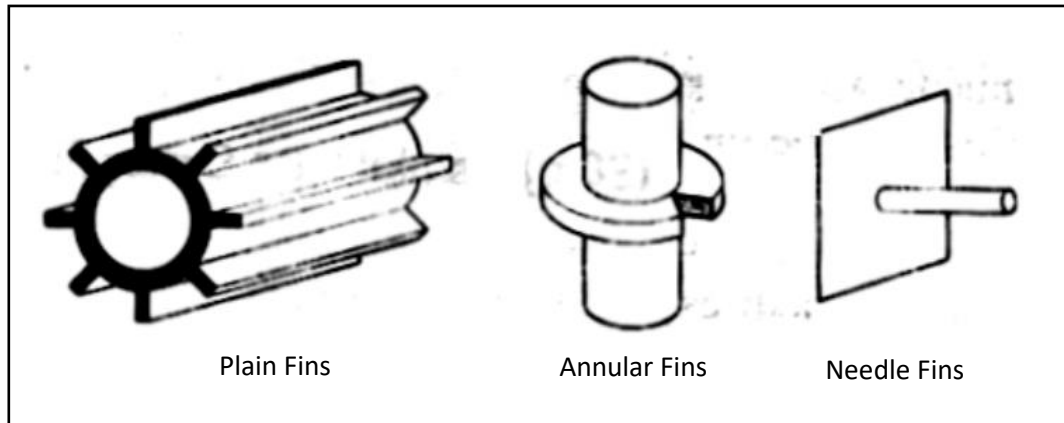


*Figure 4: Types of Fins*

In addition, fins are usually disposed in arrays, not solely. Different array configurations are possible.

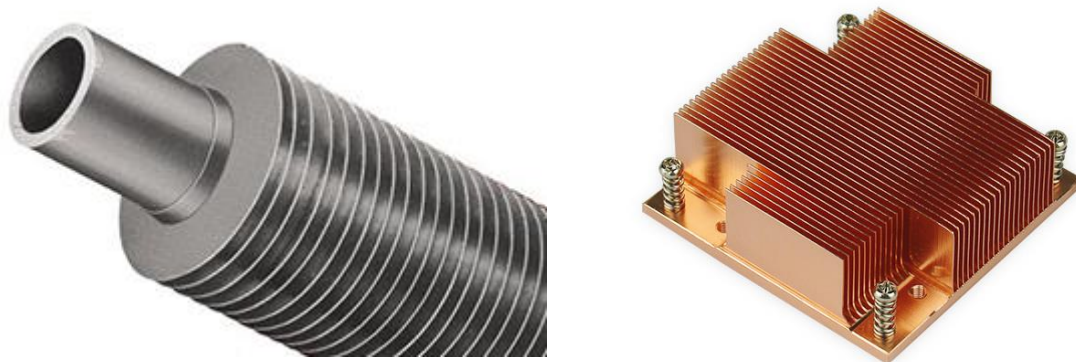


*Figure 5; Different Fin Arrays*

Before we start with deeper calculations, we should introduce some geometric parameters necessary to understand how fins are characterized.

- The base is the geometric location in which the base of the fins is placed. It has a temperature of  $T_b$ .
- Perimeter,  $P$ .
- Width,  $w$ .
- Length,  $l$ .
- Thickness,  $2\delta$ .
- Primary Surface,  $A_{kb}$ : It is calculated as the area in which convection with the air occurs, excepting the surface of the fins.
- Extended Surface,  $A_f$ : It is calculated as the area of the fins in which occurs convection.
- Fin Section,  $A_k$ : It is calculated as the section of the fin in which conduction occurs.
- Number of Fins,  $N$ .
- Parameter,  $m$ : it is calculated as  $\sqrt{\frac{hP}{kA_k}}$ .

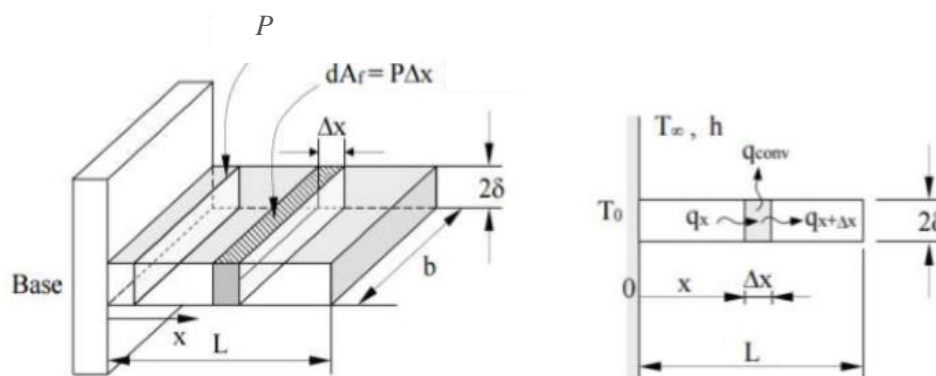


Figure 6: Fin Parameters

There are three different scenarios when studying fins: fins with adiabatic end, fins with known temperature at its end, and fins with convection at its end. Since this last scenario is the one which adequates more to reality, it will be the one objective of this study.

To simplify the problem, we can consider this fin as a fin with an adiabatic end, but with a corrected length:

$$L_c = L + \delta$$

*Equation 4*

Knowing this, the performance of a single fin compared to an ideal fin is obtained by the formula:

$$\eta_f = \frac{\tanh(mL_c)}{mL_c}$$

*Equation 5*

Once we know the performance of a single fin, we can now compute the performance of an array of fins.

$$\eta_0 = 1 - \frac{NA_f}{A_t} (1 - \eta_f)$$

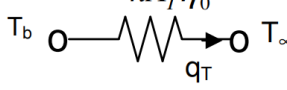
*Equation 6*

We can now introduce the concept of efficiency, which corresponds to the amount of heat we can reject with our finned surface in comparison to the heat rejected from the same surface without being finned.

$$\varepsilon_f = \frac{q_f}{hA_{kb}(T_b - T_f)}$$

*Equation 7*

Finally, to calculate the total heat transferred through our finned surface, we introduce the concept of thermal resistance. The total heat rejection is obtained as it follows:

$$R_T = \frac{1}{hA_T\eta_0}$$


$$q_T = \frac{T_b - T_\infty}{R_T}$$

Equation 8

Fins have been explained with great detail, as it is a vital component in the air-cooling systems. Moreover, they play an important role in liquid-cooling systems too, as the exchange of heat with the air is made through fins inside the radiator.

## 2.4. Liquid-Cooling Systems

It is the most extended system nowadays, as it can reject more heat than air-cooled systems. It consists of a closed circuit with a fluid inside, usually water mixed with other coolants, which takes heat from the components and exchanges it with the ambient.

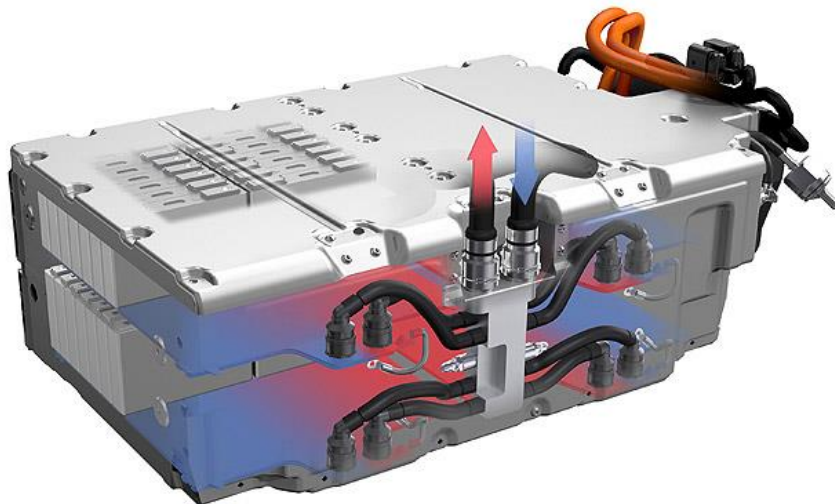


Figure 7: Example of Liquid-Cooled System

Liquid-Cooling systems are more effective rejecting heat than Air-Cooled ones, being able to stabilize temperatures in tighter ranges, independently of the ambient

temperature. It also gives the opportunity to place the heat exchanger in those places where the airflow is maximum, increasing the efficiency. However, they are more complex, heavy and expensive than its Air-Cooled counterpart.

### **2.4.1. Functioning of a Liquid-Cooling System**

The Cooling system is in charge of rejecting the heat from the batteries when they are operating. When the powertrain is turned on, the water pump starts pumping fluid through the circuit. This fluid goes around the batteries and heats up by absorbing the heat the accumulator rejects. Once the fluid leaves the heat source, it is directed to the radiator, where the heat exchange with the ambient occurs. In between, the thermostat regulates the amount of fluid that flows through the radiator, even obstructing completely the flow to achieve high temperatures faster.

### **2.4.2. Water Pump**

The main mission of the water pump is to make the fluid flow around the whole closed circuit. In electric vehicles, it is usually connected to the secondary low voltage circuit, avoiding power losses straight to the powertrain.



*Figure 8: Water Pump*

### 2.4.3. Cooling Fluid

Water is commonly used due to its economic price and its stability. However, it has some downsides that need to be taken into consideration. Water is a good electrical conductor, which can lead to fatal failures in case of a leakage inside the accumulator. Second, below 0 °C it solidifies, a condition that could make the ducts to burst. Third, at temperatures close to the boiling point is very corrosive, attacking all the metal parts in the circuit and making them to oxidize.

In order to solve these issues related to the used of water, some chemical products are added to it to decrease its freezing point below 0 °C, increase the boiling temperature above 100 °C and avoid corrosion.

### 2.4.4. Thermostat

The thermostat is the element of the cooling system in charge of maintaining the temperature of the accumulator within its operational range of temperature. When the temperature is below the desired limits, the valve regulating the fluid flow to the radiator keeps closed, making the temperature to raise quickly. When the temperature of the accumulator has reached the desired values, the valve of the thermostat opens the flow to the radiator, making the cooling system work at a steady state.

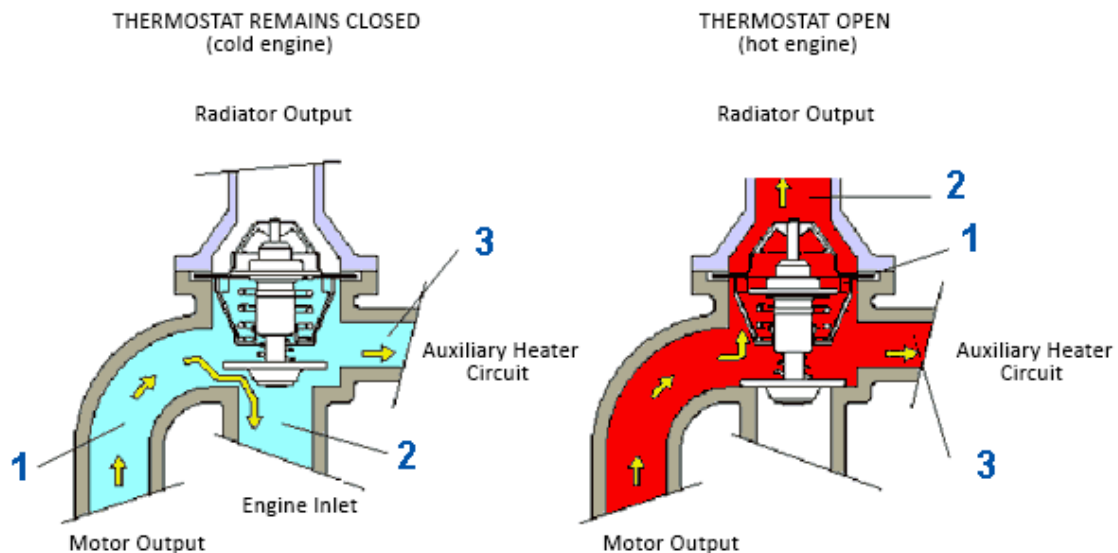


Figure 9: Thermostat

## 2.4.5. Radiator

The radiator is the component of the cooling system that exchanges the heat with the ambient air. The cooling fluid flows through it in contact with the internal fins that compose the radiator. In these fins is where the heat exchange takes place, similar to the process in Air-Cooled systems. It counts with two deposits: one for the hot water on top and other one for the cold water on the bottom. The radiator cap also works as a pressure valve, allowing excessive coolant to leave the circuit reducing pressure or permitting air to pass into it preventing vacuum in the circuit, so there are not major failures in the system.

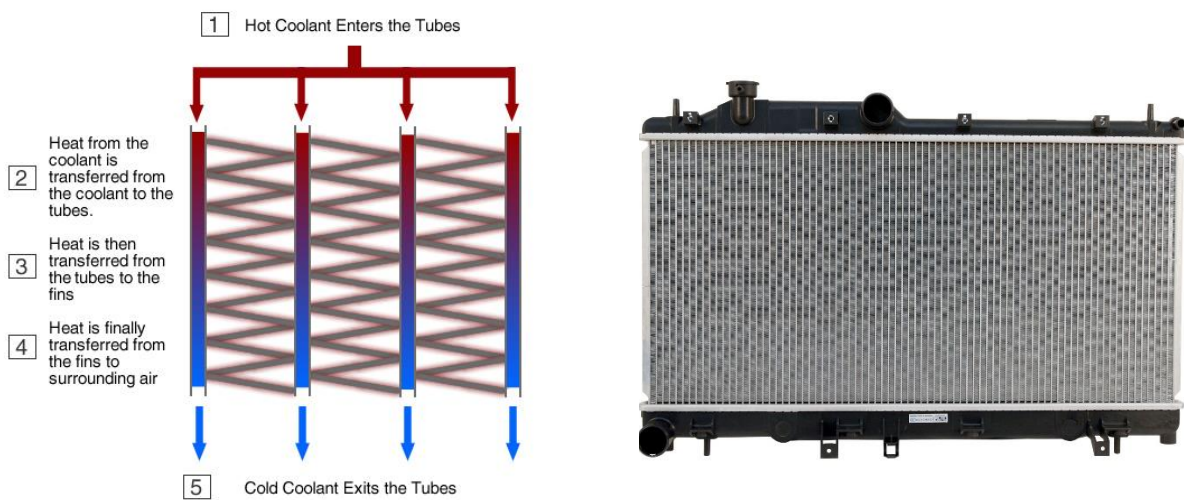


Figure 10: Radiator

## 3. HEAT SOURCES AND ASSUMPTIONS

### 3.1. Overview

A proper understanding of the heat sources and heat sinks on the vehicle will aid in choosing the most effective cooling system design. The three sources of heat under consideration are the accumulator, warm air around the drive motor, and high temperature asphalt track. The terminal heat sink will be ambient air.

The accumulator generates waste heat while charging and discharging. Electric current generates waste heat due to internal resistance of the batteries. Chemical reactions inside the battery cells also generate waste heat. The accumulator is assumed to be the major source of waste heat.

The drive motor rests just behind the driver and lies within a distance of 60 cm of the accumulator. The air around the motor was assumed to have a higher temperature due to the heat rejected by the motor. The drive motor already has a liquid cooled system to refrigerate it, so there is no need to design a cooling system for it.

The competition is held during Summer, so ambient temperatures are expected, around 35 °C, and track temperatures to be as high as 60 °C. It must be also considered radiation from the asphalt track since the accumulator lies only 10 cm above the track.

### 3.2. Accumulator

The waste heat generation from the accumulator was calculated based on a duty cycle analysis, a set of insulated discharge experiments that were conducted on single battery modules and known Lithium-ion battery properties. Battery properties that are relevant to our project can be seen in the table below.

Property	Value	Units
Nominal Voltage	3.6	V
Weight	45	G
Internal Resistance	0.02	$\Omega$
Specific Heat	1	$\text{Jg}^{-1}\text{K}^{-1}$

Table 6: Battery Data Sheet

Eight of these battery cells are connected in parallel inside a commercial battery module, designed and manufactured by Energus Power Solutions. The accumulator consists of a total of 75 battery modules connected in series. Therefore, the voltage of the accumulator is 270 V. Since the maximum power allowed to be drawn from the accumulator is 80 kW, the peak current during discharge is 296A for the accumulator, and 37A for each individual battery. Our initial model for waste heat generation was a simple model that only reflects electrical power loss due to the internal resistance of the battery cells. This equation is commonly known as the Joule’s Law. It is given by the following:

$$Q = I^2 R_{int}$$

Equation 9

Where Q is the heat rejected, I is the electrical current, and  $R_{int}$  is internal resistance. However, experimental data suggested that electrical heat is insufficient to model all of the waste heat by itself. We can see the difference between actual and modeled temperature increase, both in quantity and in tendency, in Figure 11.

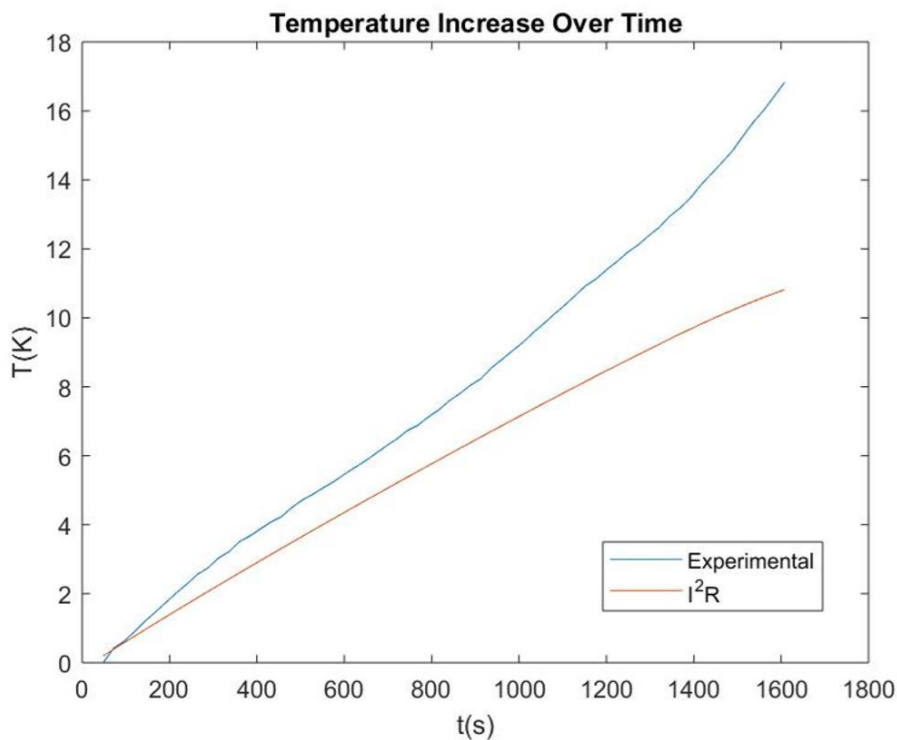


Figure 11: Initial Waste Heat Model

D.H. Jeon and S.M. Baekwhich modeled waste heat from Li-ion batteries as the combination of electrical and chemical waste heat. Equations below are the updated waste heat generation model.

$$Q = I^2 R_{int} - T \Delta S \frac{I}{nF}$$

Equation 10

$$\Delta S = nF \frac{dV}{dT}$$

Equation 11

Here  $\Delta S$  is change in entropy ( $\text{JK}^{-1}$ ),  $n$  is the number of electrons accommodating the chemical reaction, and  $F$  is Faraday's number. We could obtain a more accurate model for waste heat generation after including the term describing chemical heat conversion. The figure below compares actual data, the old model which only considers electrical power loss, and the updated model.

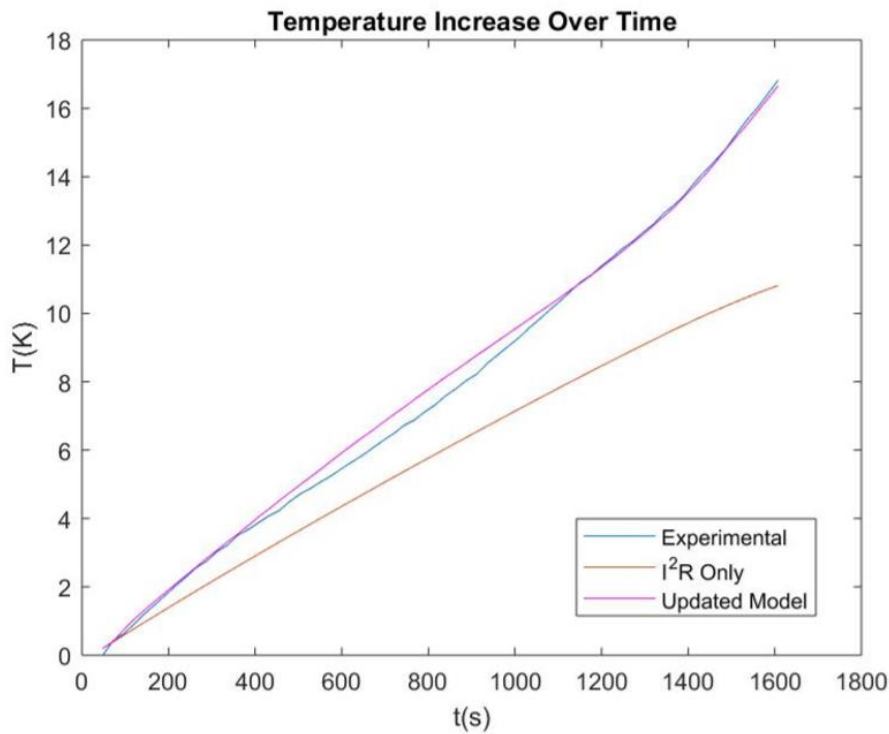


Figure 12: Updated Waste Heat Model

The updated model implies two properties. The first describes how electrical heat is quadratic to current while chemical heat is linear to current. We are able to calculate one from another based on proportionality. For example, if chemical waste heat consisted 1/3 of the total waste heat at 30A of current, it will consist 1/5 of the total waste heat at 60A. The second property is the result of chemical heat being linear to current while temperature and entropy change being independent of current. This means that the amount of chemical waste heat generated is constant given an initial and final condition of state of charge (SoC). Using this updated model, we could calculate the maximum waste heat generation rate of 16.3 kW.

Figure 13 is a sample duty cycle of the IFE vehicle that uses the low energy density accumulator. As it can be seen, the maximum current from this duty cycle is only 130 A, while the new accumulator is expected to provide a maximum current of 297 A. Since IFE has not been provided the initial and final conditions of SoC of the duty cycle, we have calculated the average waste heat by doubling current throughout the duty cycle and multiplying the result by a correction term which represents chemical waste heat. Regenerative braking is also included as a 20 A charging current during unaccelerated motion of the vehicle. The resulting average waste heat generation rate is 820 W.

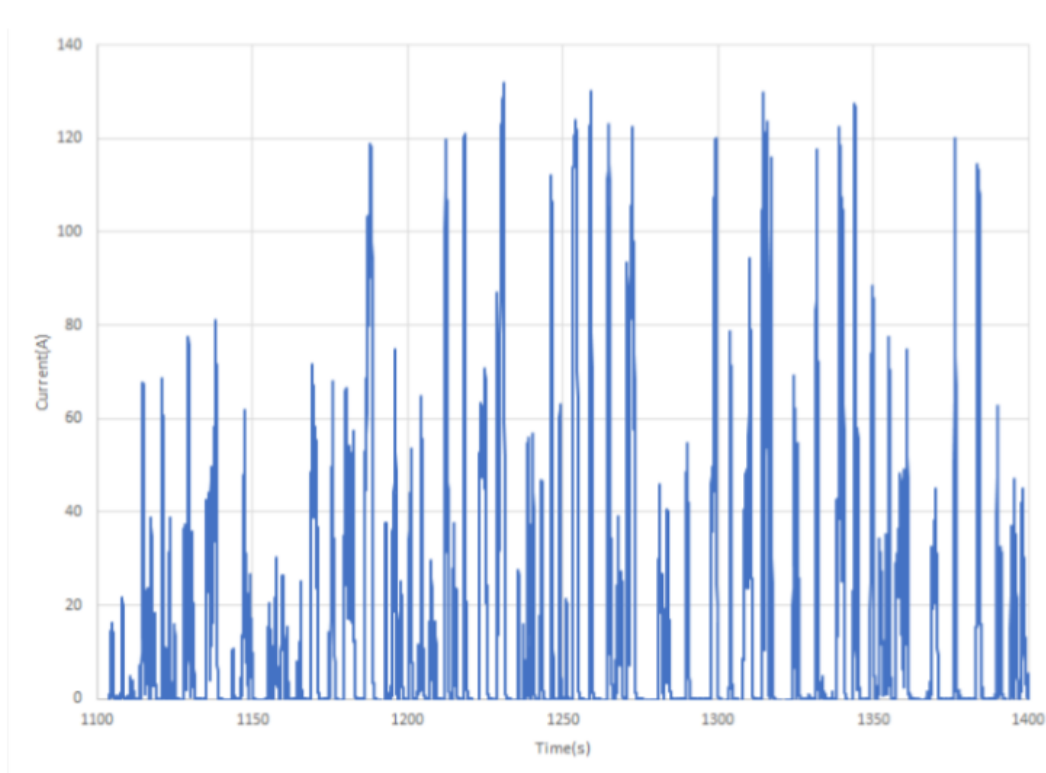


Figure 13: IFE Duty Cycle

### 3.3. Motor

Although the air surrounding the motor was identified as a potential heat source, it was determined to be negligible by IFE due to an insulating partition physically separating the motor and the accumulator.

In addition, the drive motor already has its own cooling system, so there is no need for us to take it into account when designing ours.



Figure 14: Drive Motor

### 3.4. Track

To calculate the amount of radiation from the asphalt track to the bottom of the IFE vehicle, we assumed radiative heat transfer between two infinite parallel plates. We assumed the accumulator to be at target operating temperature, 45 °C, and the asphalt to be at 60 °C. The heat transfer can be then calculated by:

$$Q = \frac{\sigma(T_1^4 - T_2^4)}{\left(\frac{1}{\varepsilon_1}\right) + \left(\frac{1}{\varepsilon_2}\right) - 1}$$

Equation 12

Where:

- Track Emissivity  $\varepsilon_1 = 0.93$
- Accumulator Housing Emissivity  $\varepsilon_2 = 0.83$
- Track Temperature  $T_1 = 333\text{K}$
- Accumulator Temperature  $T_2 = 318\text{K}$

Using the equation above, radiative heat transfer from the asphalt to the bottom of the vehicle was calculated to be 91.7 W. Since this is a small amount compared to waste heat generation from the accumulator itself, 13 kW, and due to the fact that the bottom of the vehicle will quickly convect its heat to the ambient air during vehicle operation before conducting it to the accumulator, this factor will be disregarded in further analysis.

## **4. PROPOSED CONCEPTS**

### **4.1. Brainstorming**

After brainstorming possible cooling methods, feasible concepts were narrowed based on energy efficiency, weight, cost, and competition regulations. The different options were chosen from the sponsor's catalogue. Since our task was to increase heat transfer from the accumulator to the ambient by transferring heat from inside the accumulator to the ambient air sink, solutions with complex geometries and which only could transfer heat in relatively shorter distances were dismissed. The concepts that made it to the final stage and discussion are the ones that follow.

### **4.2. Fins and Heat Pipes**

Fins are one of the most commonly implemented methods of increasing heat transfer. Fins operate by increasing surface area, allowing for a larger heat transfer surface. By attaching these to a heat source, the increase of surface area draws the heat away from it and cools the epicenter. Fins are passive cooling devices, designed to increase convection regardless of flow rate of air, thus they will affect the vehicles aerodynamics. Through optimization of fin efficiency considering the geometry and the material of the fin, we are seeking to build a fin structure that will effectively transfer the heat from the accumulator to the ambient, lightweight, and causes least drag. In addition to this fin structure, we can implement heat pipes that are interlocked with these fins to reject even more heat. To combine the heat pipes and fins, heat pipes will be located between the battery packs. Novark Technologies has a vast amount of different heat pipes in which we could utilize to cool the accumulator. An example of how fins and heat pipes can be implemented is depicted in Figure 15.

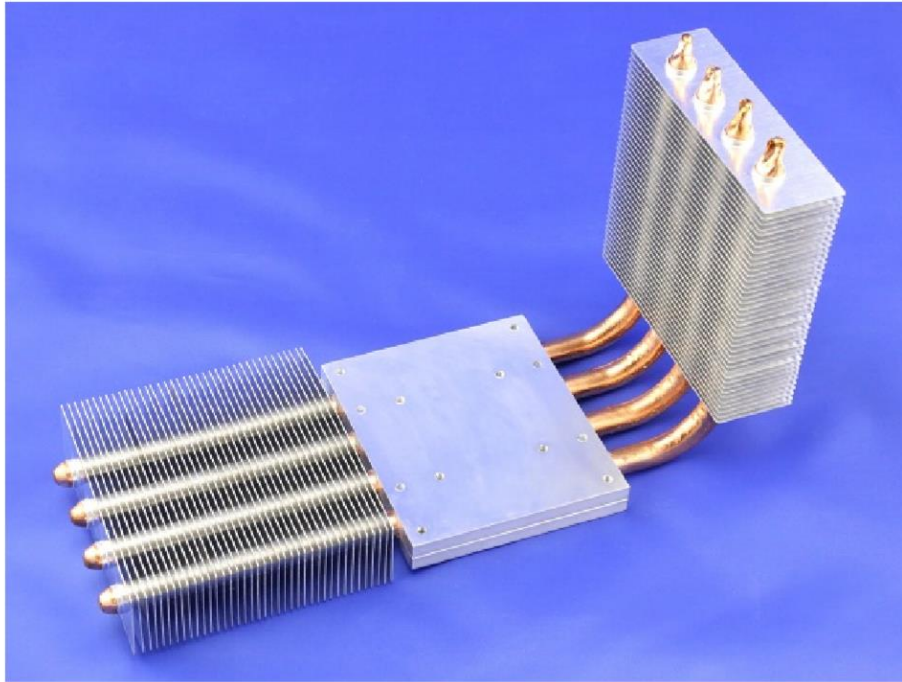


*Figure 15: Fins and Heat Pipes*

### **4.3. Vapor Chambers**

Vapor Chambers are being also considered as a concept due to their compact structure. They are similar to heat pipes but are not affected by orientation. They are constructed from thin copper sheets with a hollow chamber, and they are frequently employed as heat sinks in the CPU and GPU cooling systems. Liquid at the contacting surface will absorb the heat, evaporate, and carry away the heat in an endothermic reaction. The vapor then condense on the top layer of the chamber in an exothermic reaction and reject heat into the air. It can create a uniform bed of temperature at the surface. Their main advantage is a low weight and thin geometry, allowing us to place them in critical points that are not accessible. An even temperature curve can be achieved through the entire accumulator by inserting thermal pads between the flat vapor chamber surface and the battery cells, creating an ideal operating environment. This can be achieved placing more vapor chamber where the temperatures are expected to be higher. “However, the custom built chambers are made of expensive materials and have a high prototyping cost. A typical vapor chamber from Novark can be seen below in Figure 16.

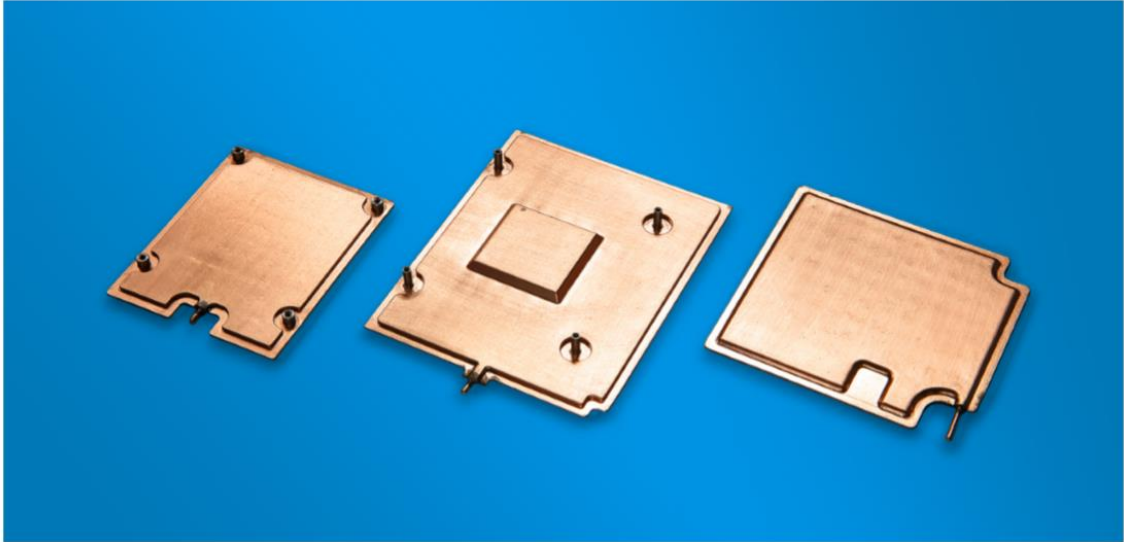


*Figure 16: Vapor Chambers*

#### **4.4. Vacuum Brazed Cold Plates**

Vacuum Brazed Cold Plates are constructed by brazing two metal plates in a vacuum environment. Working fluid will be pumped between the plates and act as an active coolant. Fins will also be inserted between the plates to maximize the heat transfer. The plate will be placed on the bottom of the accumulator to increase the contact area with air. This active system is the most effective way of cooling the accumulator, but it is also the most expensive of all the concepts in consideration. In addition, as it is the only active system among the ones we have short-listed, overall car efficiency can be compromised as it needs an external source of power, so it is necessary to balance the gains in cooling with the energy losses through the water pump. To improve the efficiency of the vacuum Brazed Cold Plates, heat pipes can be embedded, so the passive heat transfer of the system increases. Another potential problem is that this will be placed in the coolant flow downstream the motor and other heat sources already refrigerated, being then necessary a larger cooling system. A sample vacuum brazed cold plate can be seen below in Figure 17.



*Figure 17: Vacuum Brazed Cold Plates*

#### **4.5. Loop Heat Pipes**

This concept is a continuous heat pipe, where the two-phase fluid only goes in one direction. As sections 4.2 and 4.3, it is a passive system, eliminating the need for external power. The main advantage of this concept is that allows to eject the heat in a remote location from the heat source thanks to the length of the continuous pipe. In a car this can be very useful, as you can eject the heat there where the air flow is at a maximum, increasing the efficiency of the system. Unfortunately, the Loop Heat Pipe is a new prototype technology, so its benefits and drawbacks are not certain. This can be a great opportunity for our sponsor to test it, thus we are further exploring this option with our sponsor to determine its viability. The loop heat pipe from Novark can be seen below in Figure 18.

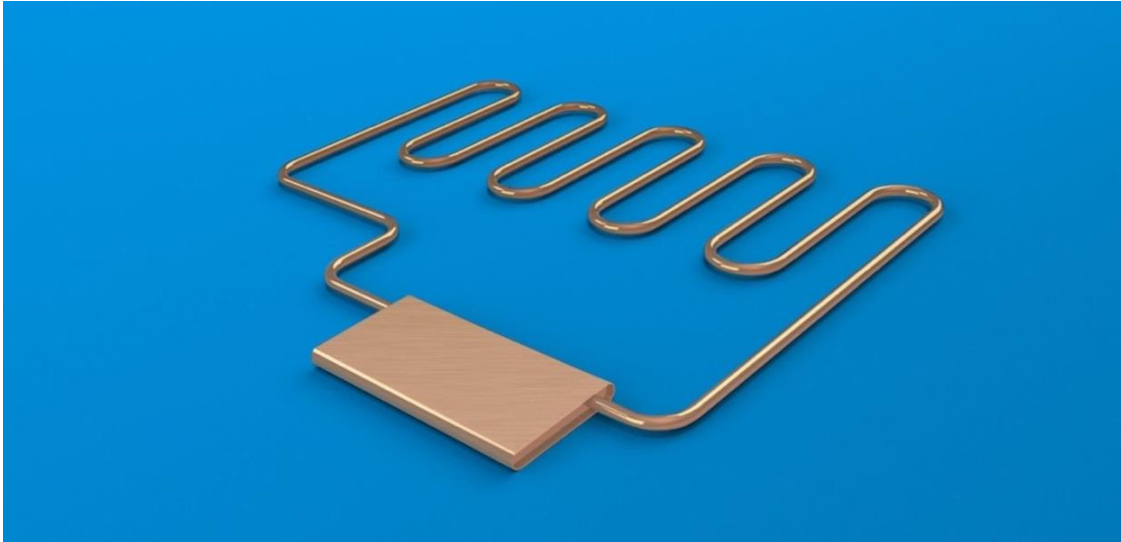


*Figure 18: Loop Heat Pipe*

#### **4.6. Complementary Concepts**

Two additional concepts were also determined to be possible. However, due to the nature of their capabilities, it was decided that these would rather be implemented alongside as complements to the concepts discussed above. The first of the ideas is the use of dry ice. Dry ice, at a temperature of  $-78.5\text{ }^{\circ}\text{C}$ , would be extremely useful to cool down the airflow or fluid flow coming into our heat transfer concepts. With this colder inlet, much more heat could be transferred to the working fluid. However, this concepts drawback is that dry ice will only last temporarily before complete vaporization. The second complementary concept is the use of parafin wax. Illini Formula Electric has received tubes of paran wax that can be heat shrunk around the batteries. A phase change would occur when the wax was melting under heating. This would keep the batteries at a constant temperature until the wax was completely melted. This most likely cannot be used on its own, however, because the wax will likely melt before the approximately 45 minute endurance run would finish. When used in conjunction with a concept such as heat pipes, the wax could keep a constant temperature during the shorter acceleration runs, while the heat pipes could transfer heat away from the batteries during an endurance race in which the vehicle would be driven more conservatively resulting in a lower heat output for the heat pipes to transfer.



## **5. CONCEPT DEVELOPMENT AND INITIAL DESIGN**

Some of the initial concept designs that we looked into included vapor chambers, vacuum brazed cold plates, and loop heat pipes in addition to traditional heat pipes.

Vapor chambers are similar to heat pipes but are not affected by orientation. They are constructed from thin copper sheets with a hollow chamber and are frequently employed as heat sinks in the CPU and GPU cooling systems. However, vapor chambers were too expensive and too thick for our application.

Vacuum brazed cold plates are constructed by brazing two metal plates in a vacuum environment. Working fluid will be pumped between the plates and act as an active coolant while fins are inserted between the plates to maximize the heat transfer. We have disregarded cold plates as a viable option since it was a liquid cooling system, after IFE suggested that they were not willing to redesign the water pump they were using to cool the drive motor.

The loop heat pipe is a continuous heat pipe, where the fluid and vapor each circulate around the pipe in opposite directions. It allows for the remote rejection of heat. However, the development of the loop heat pipe is still in prototype stage. This implies that it is likely to encounter unexpected complicated problems in the actual implementation.

Considering cost, performance, and stability, a design consisting of heat pipes and fins was chosen. This cooling system utilizes both conduction and convection to reject the unwanted waste heat from the accumulator to ambient air. As stated before, the expected primary source of waste heat will come from the battery modules. The heat sinks will provide heat transfer through conduction by being placed in between each inner battery module, so there will be a total of 14 heat sinks for each row. The waste heat will then be transferred to a series of three heat pipes in staggered configuration perpendicular to the air flow. Flat annular fins shall be assembled onto each heat pipes. These fins will then transfer the waste heat through forced convection, which is aided by fans attached to the accumulator housing.



## 6. ANALYSIS

### 6.1. FEA Simulations

In order to validate our cooling system design, we performed FEA simulations for conductive heat transfer with Abaqus. The results of the simulations were then used to calculate the thermal resistance from the cell surface to the heat pipes inserted into the heat sinks. We assumed an effective thermal conductivity that accounts for the overall heat transfer characteristics of the heat pipes. Since the license for Abaqus available did not allow the use of extensive features such as the usage of heat generation as a boundary condition and the usage of more than 10,000 meshes, two different simulations were modeled to obtain the desired results.

We modeled the contact interface between the battery and the heat sink as two square blocks with a contact surface in between. Material properties of a Li-ion battery were assigned for the square structure on the left while properties of aluminum 6061 were assigned for the square structure on the right. Additionally, the contact interface between the two square structures was modeled as a 1mm thick layer of thermal paste, which has a thermal conductivity of  $2 \text{ Wm}^{-1}\text{K}^{-1}$ . Heat transfer rate used for this simulation was calculated on the assumption that the entire accumulator generates 5000 W of waste heat uniformly. The temperature of the rightmost edge of the square structure on the right was designated to be  $40 \text{ }^\circ\text{C}$ . The temperature increase due to conduction can be seen in Figure 19.

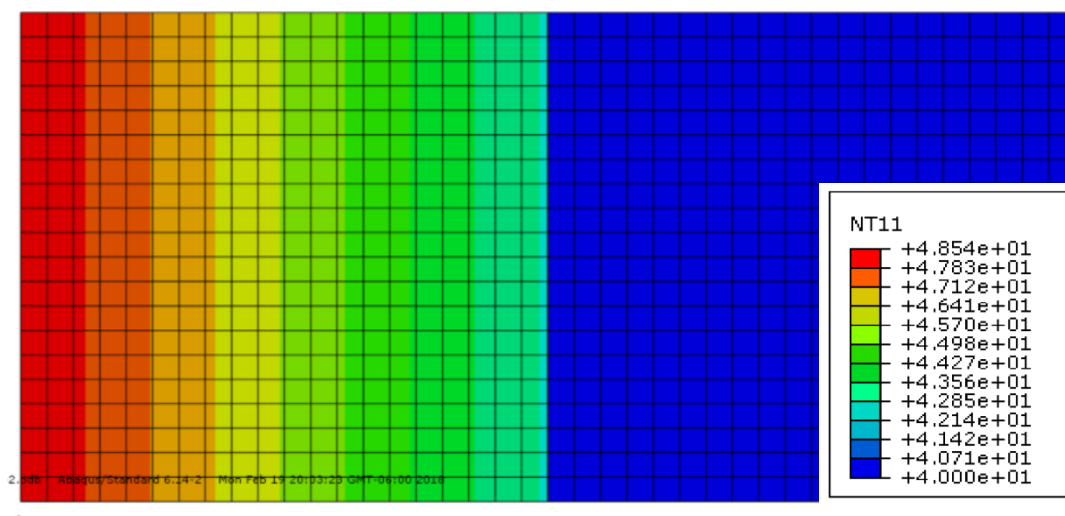


Figure 19: Interface Simulation

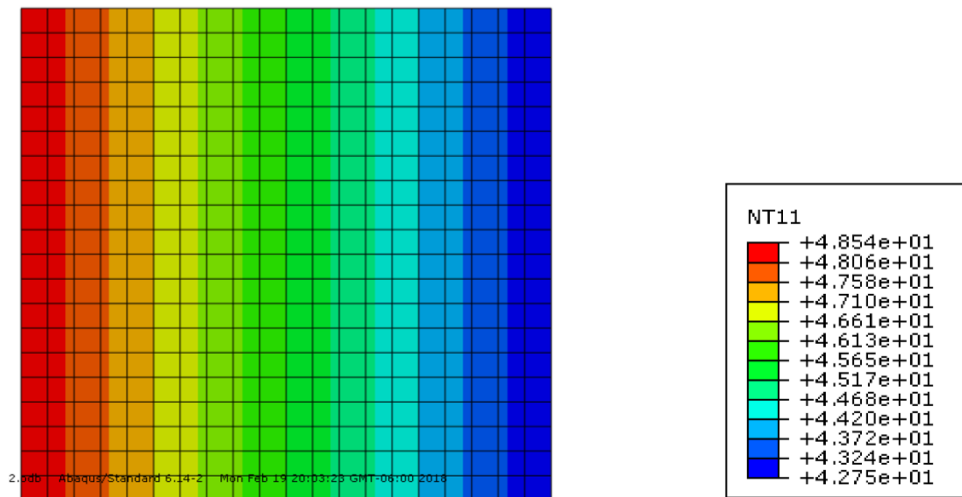


Figure 20: Interface Simulation, Battery Side

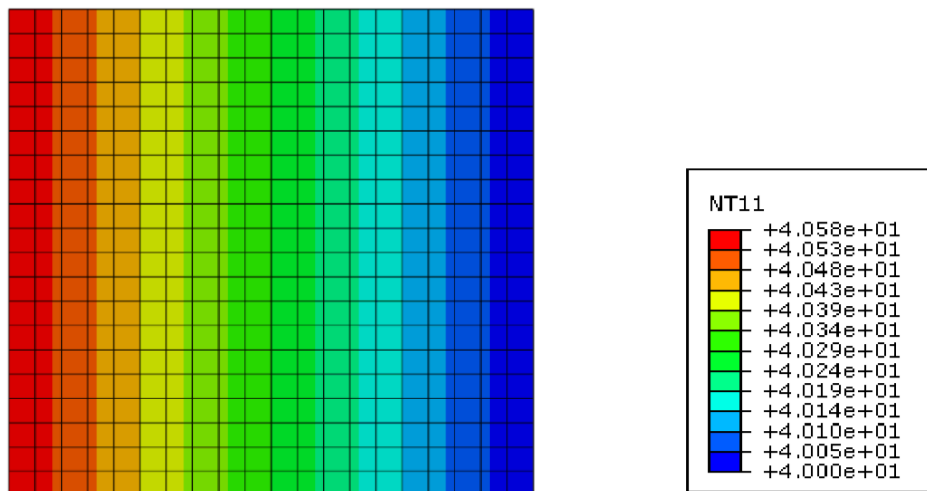


Figure 21: Interface Simulation, Heat Sink Side

Figure 22 shows the simulation result for the heat sink and heat pipe components. The wing-like structure with curved surfaces are heat sinks assigned with the material properties of aluminum 6061, which is same as the right hand side square structure from the former simulation. The vertical structure in the middle represents heat pipes and was assigned a thermal conductivity of  $10000 \text{ Wm}^{-1}\text{K}^{-1}$ . This number is the minimum effective thermal conductivity of a heat pipe suggested by our sponsor Novark Technologies, Inc. The boundary conditions for heat transfer were unchanged from the previous simulation. The temperature of the tip of the heat pipe structure was designated to be  $40 \text{ }^\circ\text{C}$ .

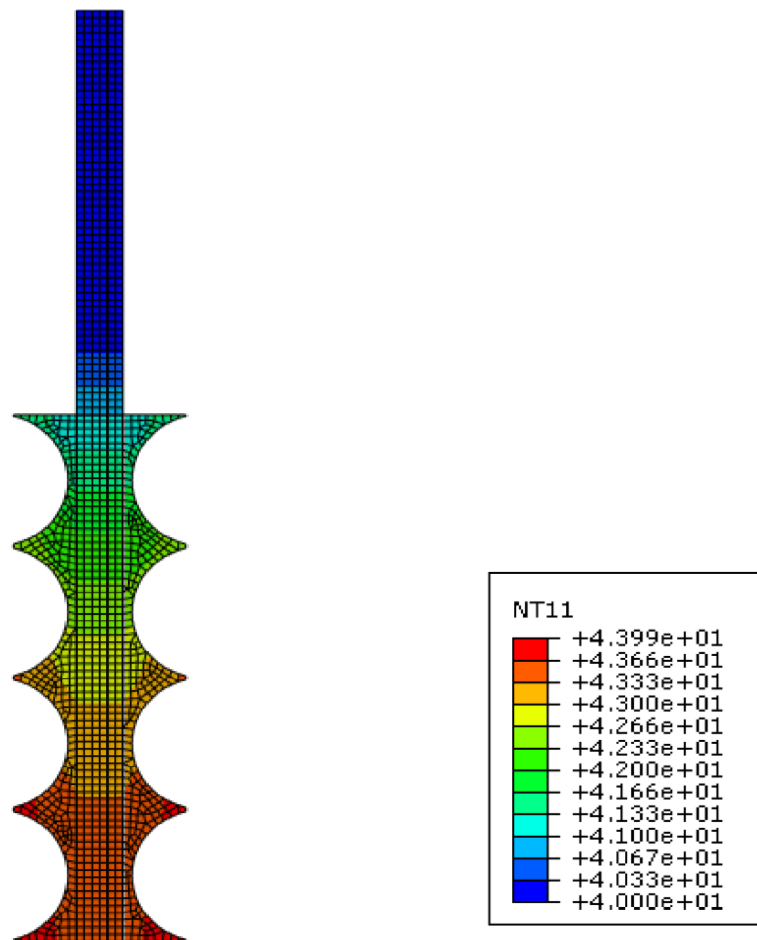


Figure 22: Temperature Profile

We could calculate the thermal resistance along the path of conduction based on the simulation results to be  $1.23 \times 10^{-3} \text{KW}^{-1}$ .

$$R_{th} = \frac{\Delta T_{cond}}{Q}$$

*Equation 13*

Here  $R_{th}$  is the thermal resistance ( $\text{KW}^{-1}$ ) and  $\Delta T_{cond}$  is the temperature difference along the path of conduction. This allows us to calculate the temperature difference between the battery surface and the tip of the heat pipes for a given heat transfer rate of the accumulator. For example, the temperature difference for our average waste heat generation rate was  $1.009 \text{ }^\circ\text{C}$ .

## **6.2. Air-side Heat Transfer**

The fin array was analyzed and designed by using convective heat transfer models which utilize the Colburn j factor. Initially, annular flat plate fin arrays were chosen due to their computational simplicity. The Colburn j factor for that geometry is given by the equation below.

$$j = StPr^{2/3} = 1.745Re_h^{-0.4}W^{-2/3}R_b^{-0.4}K_{z,h}$$

*Equation 14*

Two simultaneous equations were solved, one representing heat rejected by fins and the other representing the heat absorbed by air, to obtain the outlet air flow temperature and the overall heat rejection from the fins to ambient air.

$$Q = h_{conv}NA_h\eta_0(T_b - T_0)$$

*Equation 15*

$$Q = \rho V_{air} A_f C (T_0 - T_i)$$

Equation 16

MATLAB was used to obtain numerical solutions of the equations. Geometric parameters of the fin array, such as fin length, fin pitch, and fin thickness were varied to optimize performance. Results of this optimization process are plotted and tabulated on Figure 23 and Table 7, respectively. They indicate that the heat transfer is highest when the fin length is maximized and the fin spacing is 1 mm while the fin thickness is 0.2 mm. The resulting outlet temperature is 41 °C and heat transfer is 1007 W for the entire accumulator. The outlet temperature is below the target 45 °C and the heat transfer value was 1.23 times the expected average heat transfer.

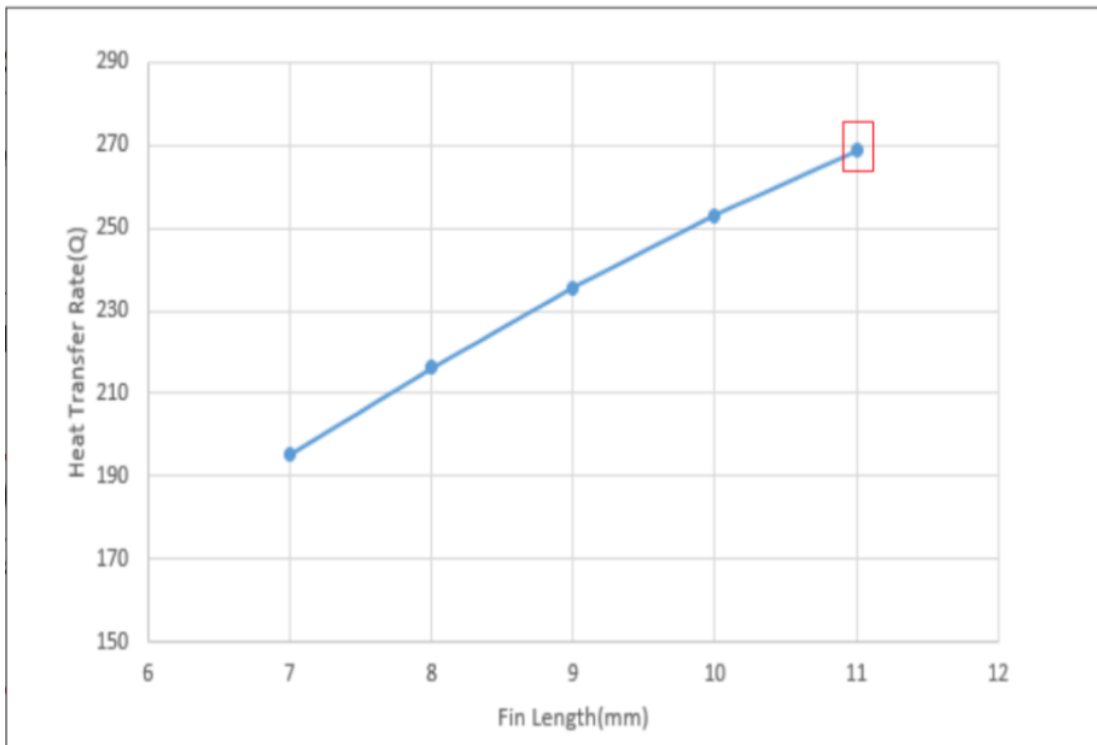


Figure 23: Heat Transfer Rate vs Fin Length

		Spacing(mm)				
Thickness(mm)		0.5	1	1.5	2	2.5
	0.1	376.28	316.19	277.91	251.02	230.97
	0.2	374.38	325.34	291.69	266.94	247.86
	0.3	364.62	323.24	293.23	270.5	252.6
	0.4	353.6	318.28	291.31	270.35	253.58
	0.5	342.68	312.41	288.06	268.69	252.95

Table 7: Heat Transfer Rate vs Fin Spacing and Fin Thickness

Despite having the annular fin array meeting our cooling requirements, we switched to rectangular flat plate fins for manufacturability. The fins shall be manufactured and assembled into the prototype by our sponsor. They recommended a fin thickness of 0.5 mm and a spacing of 2 mm, which would be easiest for them to fabricate in a short time period. In order to verify the performance of the new geometry, we repeated the analytical calculations with the Colburn  $j$  factor for rectangular flat plate fins.

$$j = 0.108 Re_{D_c}^{-0.29} \left(\frac{P_t}{P_1}\right)^{P_1} \left(\frac{F_p}{D_c}\right)^{-1.084} \left(\frac{F_p}{D_h}\right)^{-0.786} \left(\frac{F_p}{P_t}\right)^{P_2}$$

Equation 17

According to the paper written by C.C Wang et al., on which this correlation was developed, this may only be applied to a single row of flat plate fins on tubes. Our design has a large gap in between each array of fins so we assume that the flow would stabilize by the beginning of the next row. MATLAB code was used to iterate over the 15 rows to obtain an outlet temperature of 41 °C and a heat transfer of 983 W, 1.2 times the average expected.

### **6.3. CFD Simulations**

Our heat transfer calculations were confirmed by comparing the same to a CFD simulation of our design, provided by Novark Technologies. In the simulation, a constant volume flow rate of 200 CFM was applied at the inlet of the model and atmospheric pressure was applied to the outlet of the model, shown in Figure 24. In this simulation, each battery cell was set to be a heat generation source of 20 W. The maximum temperature obtained in this simulation was at the battery cell surface of 47 °C. This is 2 °C higher than the target temperature of 45 °C. Since waste heat generation of 20 W per battery cell is nearly double the amount of our expected average waste heat generation of 11 W, we are confident that our design can keep the temperature under 45 °C in actual operation.

The maximum pressure drop was over 1600 Pa. However, this only occurred when the airflow was directly obstructed by the battery surfaces. The pressure drop along the fin arrays were 900 Pa, which can be overcome by fans.

A simulation was also conducted for the worst case waste heat generation with each battery cell modeled to generate 176 W instead of 20 W but only for 10 seconds. This was done to account for the acceleration spikes in the duty cycle of the endurance event and the entire duration of the acceleration event. Other boundary conditions were maintained for better comparison. The simulation results can be seen in Figure 25. The maximum temperature reached was 41 °C. This shows that even when under the maximum acceleration, battery temperature will not exceed our design margins, as long as the duration is short. In order to compensate for this duration limit, phase change material will be used in the vacant holes of the heat sinks.

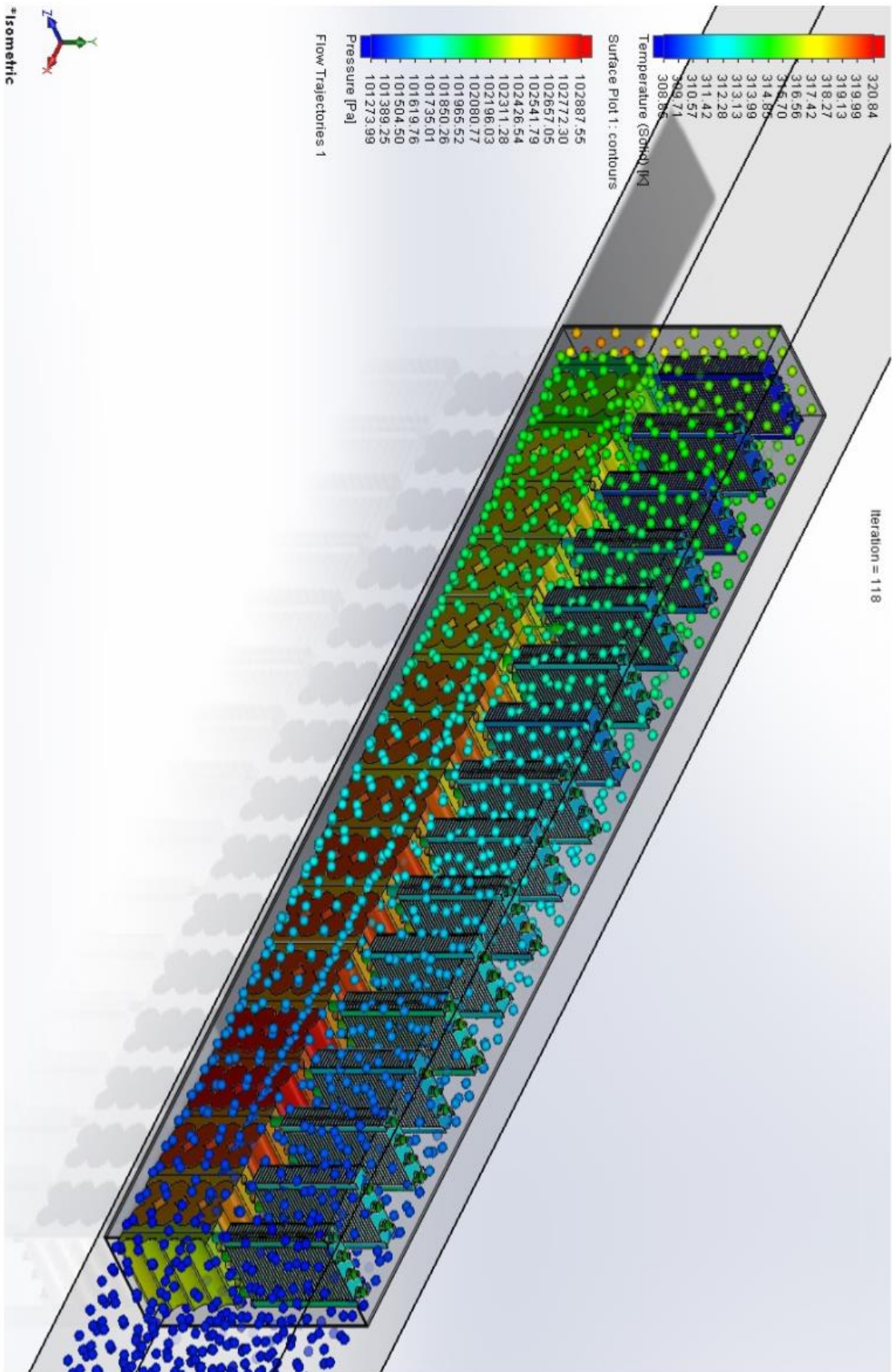


Figure 24: Steady State Pressure Drop Simulation

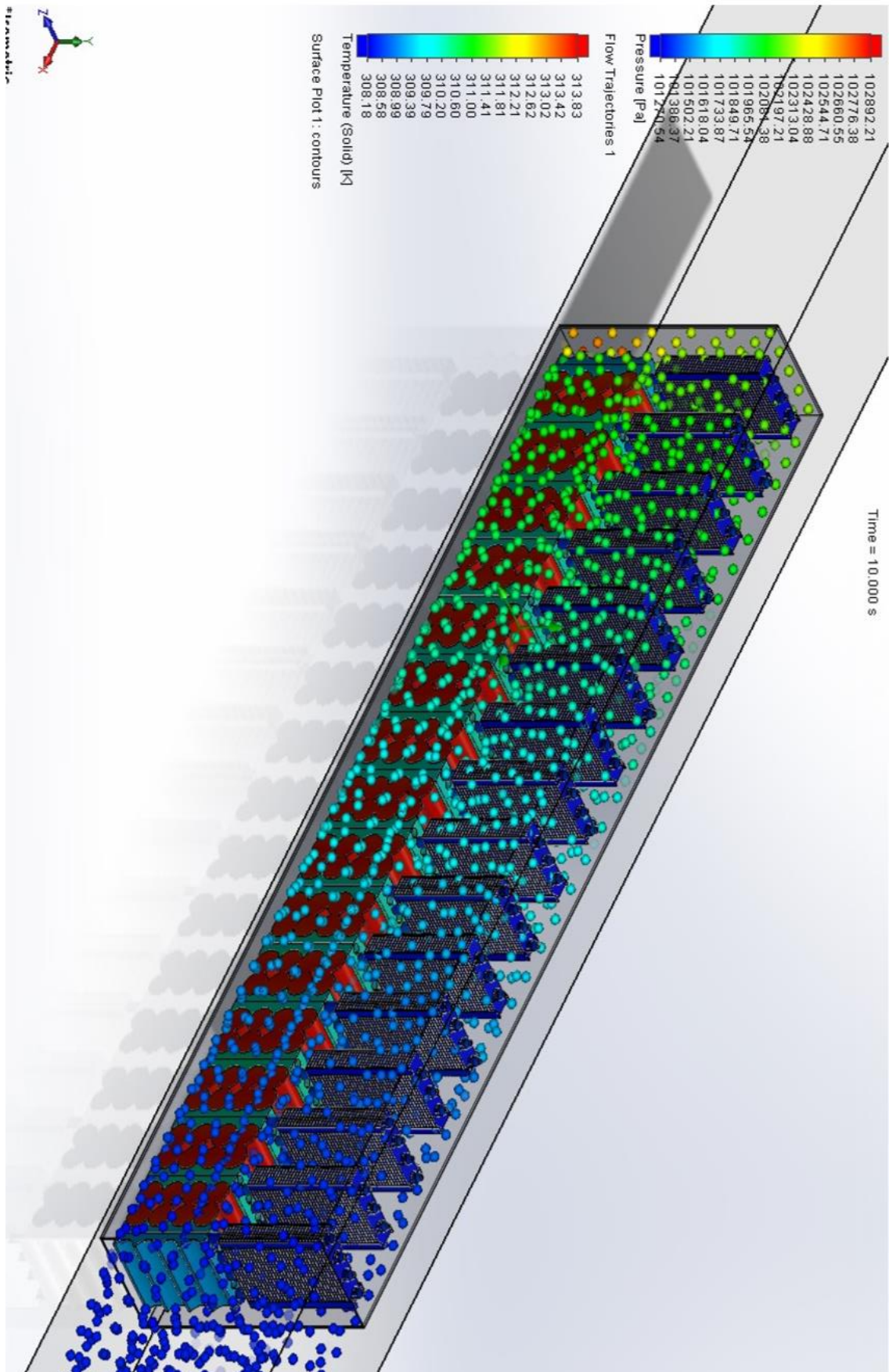


Figure 25: 10 s Pressure Drop Simulation



## 7. EXPERIMENTS

### 7.1. Battery Module Waste Heat Generation Experiment

An insulated discharge experiment was conducted in order to confirm our initial waste heat generation model that only takes into consideration electrical power loss. The resulting mathematical model from this experiment is provided in Section 3.2. For the experiment, we used Li-ion Building Block Li8P25RT designed and manufactured by Energus Power Solutions. A CAD model of the battery module is shown in Figure 26.

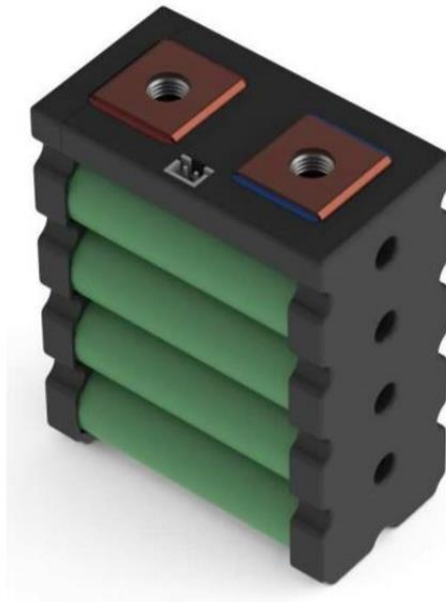


*Figure 26: Battery Module*

Each battery module has a 4-point temperature sensor embedded in the four negative poles of each two adjacent cells which can be connected to an external circuit with a JST XH 2 pin connector. We will be using this sensor to measure temperature for the experiments. The battery module operates at a nominal voltage of 3.6V, a maximum voltage of 4.2V, and an average capacity of 20 Ah. The sensors utilize a temperature variable voltage shunt reference, which acts as a Zener diode with its voltage drop depends sensitively on its temperature. In order to measure the output of the external temperature sensor connectors, a pull-up resistor of approximately  $680\Omega$  must be connected between the cathode of the battery and the cathode of the diode, while the

anode of the battery is connected directly to the anode of the diode. The circuit diagram is shown in Figure 27.

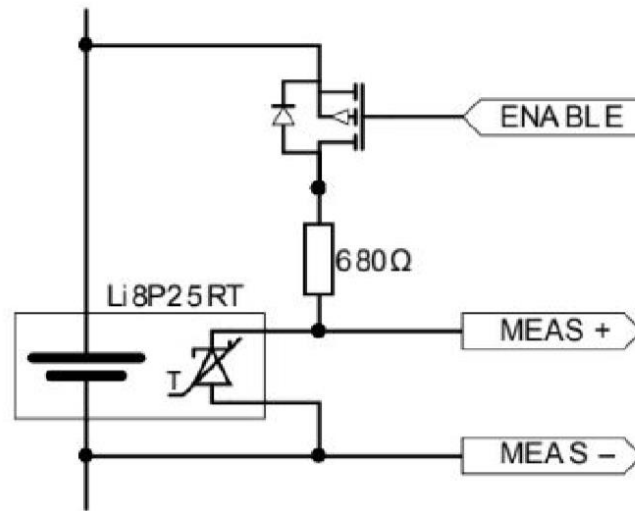


Figure 27: Sensors Circuit Diagram

In this experiment, an initial current of approximately 33A was drawn. The equipment we used includes a  $0.1\Omega$  power resistor (Euro-Power Wirewound, EVRT170ENR10KE), 12 gauge vehicle wire (McMaster-Carr, 6659T28) that is capable of handling a maximum of 38A of current, a vertical lever actuator (McMaster-Carr, 7110K24) for high current purpose, and lugs (McMaster-Carr, 7980K31) for battery terminal connections. A customary  $680\Omega$  pull-up resistor is connected to the sensor to prevent excessive current that will damage the sensors. NI USB-6009 was used to measure the potential difference, FLIR ONE Pro thermal camera to record the infra-red image of the battery module to determine the uniformity of the surface temperature, and Omega RDXL4SD thermometer with 4 probes to measure temperatures at specific points on the battery surface for data acquisition.

A simple experimental setup consisting of one battery module connected in series with a  $0.1\Omega$  power resistor and a vertical lever actuator is shown in Figure 28. Note that we insulated our battery module using wood board, which is a good thermal insulator. This will emulate the battery module boundary conditions inside the actual accumulator.

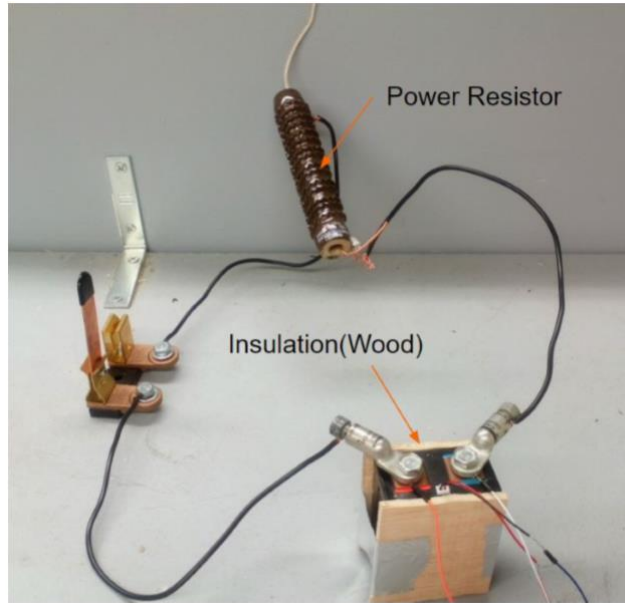


Figure 28: Experiment Setup

The actuator acts as a switch which is a safety mechanism that allows us to disconnect the circuit at any point in necessary. Additionally, it allows us to connect the circuit at a specific moment, so data recordings can be synchronized. Potential difference across the battery module, the power resistor, and the temperature sensor was also measured. When the current started to flow through the circuit, thermal images of the battery were collected to identify potential hotspots on the battery surface. A picture of the thermal image of the battery module is shown in Figure 29.



Figure 29: IR Camera Picture

According to Figure 29, the battery module surface temperature is uniform across the curved surface of each cell and validates our assumption that the temperature is the same in the longitudinal direction of the battery cells. Therefore, we can put the four thermocouple probes at the center of each battery cell at one side of the module. The temperature converted from the sensor voltage output differential and the average temperature outputs from the four thermocouple probes are plotted below in Figure 30.

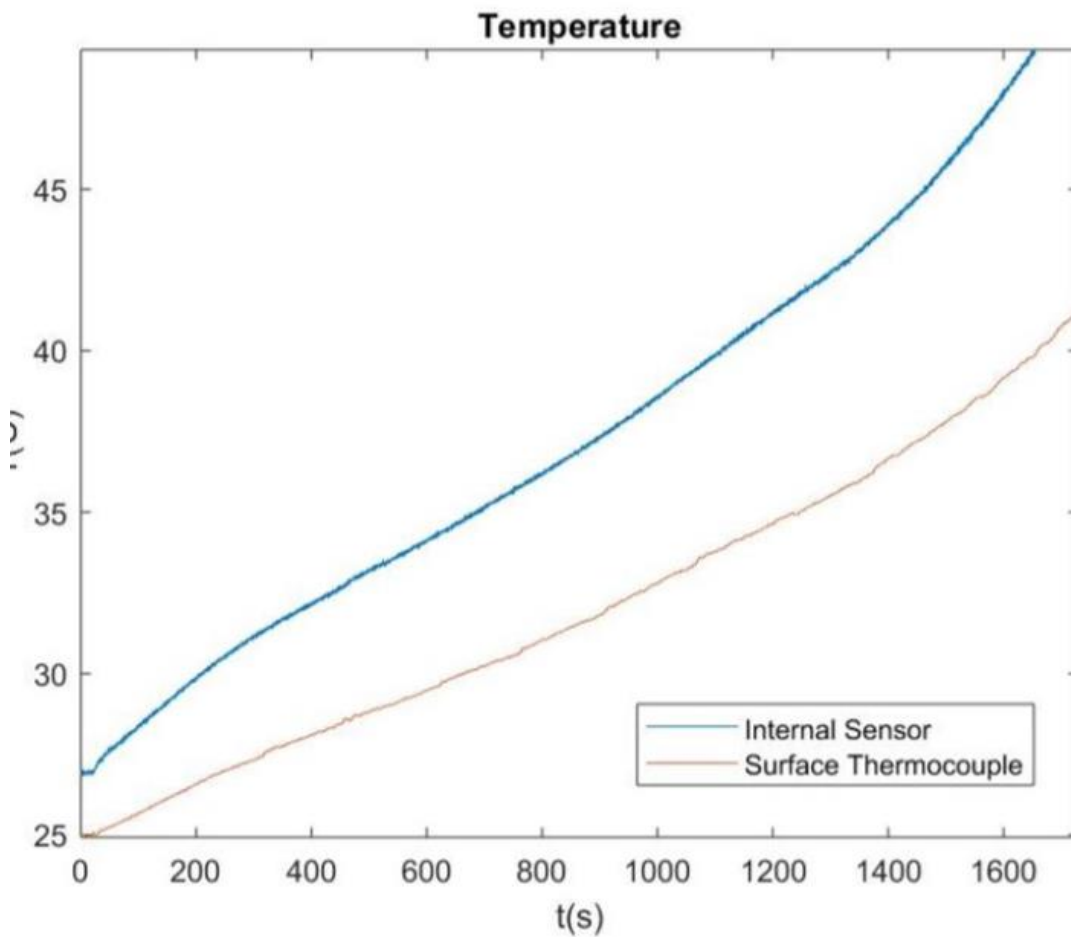


Figure 30: Sensors and Surface Temperature

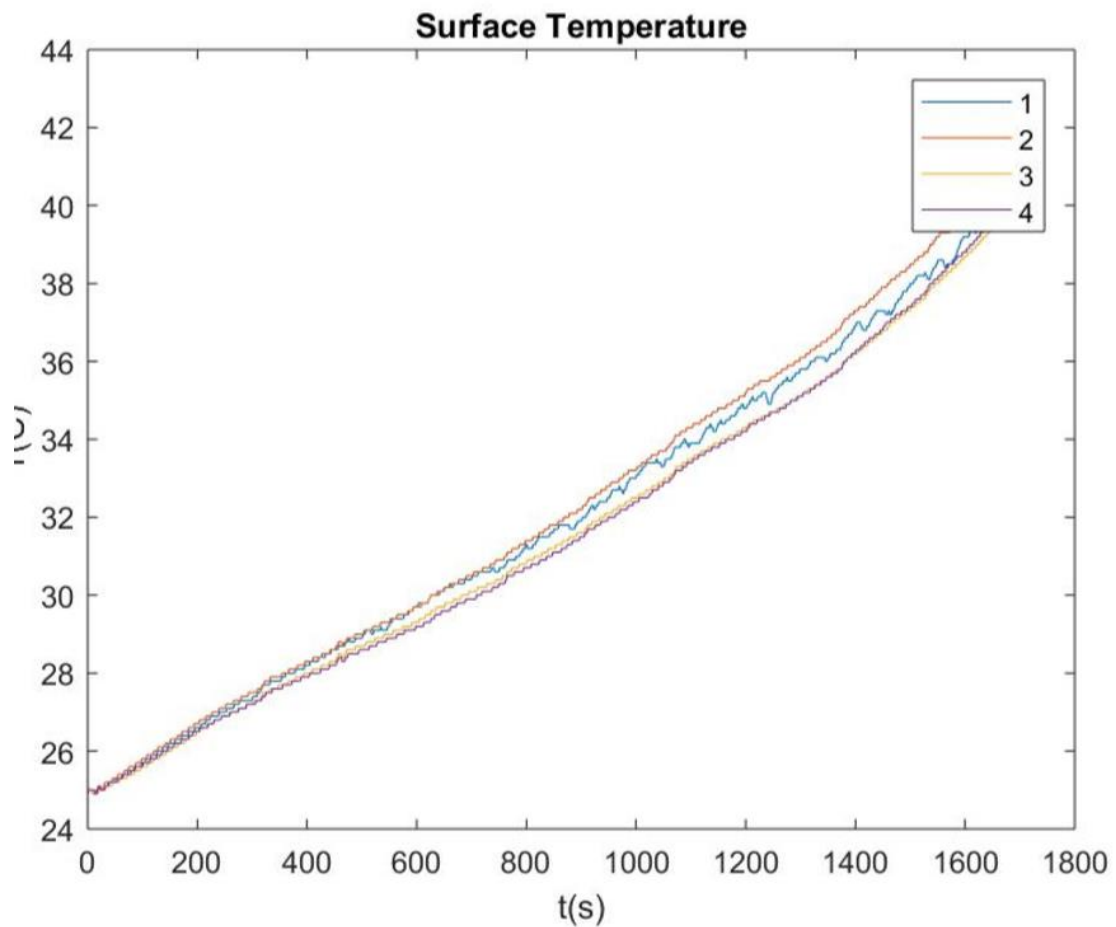


Figure 31: Surface Temperature for Different Batteries

## 7.2. Pressure Drop Experiment of Four Fin Arrays

Wind tunnel testing was conducted to validate the pressure drop simulated by our CFD model. The wind tunnel was made available by our faculty advisor, Professor Anthony Jacobi, with a variable inlet flow velocity capable of up to  $7\text{ms}^{-1}$ . Since the actual prototypes are currently being manufactured, we created a replica of the fin geometry to conduct this experiment. Fins were water jet cut from a thin aluminum sheet, and were placed inside 3D printed alignment brackets to ensure 2 mm fin spacing. In addition, wooden rods of 6 mm diameter were inserted through the fin holes to imitate the geometry of heat pipes. The assembly of fins, rods, and brackets were glued to a wooden

air duct so that there was no gap between the fins and the duct wall for the air to bypass through. The experimental set up can be seen below in Figure 32.



*Figure 32: Pressure Drop Experiment Setup*

The pressure transducer available at the wind tunnel could not measure pressure that is higher than 125 Pa, we filled a U-shaped tube with water and connected it to the inlet and outlet of the air duct to use it as a manometer. The difference in height of water inside the tube manometer is converted to pressure.

$$\Delta P = \rho gh$$

*Equation 18*

A target pressure drop of 240 Pa for 4 fin arrays was set, which corresponds to 900 Pa for 15 arrays, assuming that the pressure drop increases linearly as the number of arrays increases. This value was chosen in order to match the pressure drop with the value obtained through simulation. The objective of this experiment was to check the air flow rate at that specific pressure drop. At a pressure drop of 240 Pa a flow rate of 45 CFM was observed.

Combined with the CFD simulation results at 200 CFM and 900 Pa, this implies that the duct dimensions can be controlled to achieve an air flow rate that is between 180 and 225 CFM and a heat rejection rate that is at least 983 W while maintaining the pressure drop at 900 Pa.



## 8. FINAL DESIGN

### 8.1. Heat Sinks

The heat sinks shall be manufactured with Aluminum 6061, which is low cost and easy to manufacture. This material also has a high thermal conductivity of 151 to 202  $\text{Wm}^{-1}\text{K}^{-1}$ . The heat sinks have a curved surface geometry to insure perfect contact with the battery surfaces, which can be seen below in Figure 33. Additionally, a thin layer of thermal paste with a thermal conductivity of 2  $\text{Wm}^{-1}\text{K}^{-1}$  will be applied on the contact interface between the battery and the heat sink. This will minimize the amount of air in between small gaps of the interface. Since air has a thermal conductivity of approximately 0.03  $\text{Wm}^{-1}\text{K}^{-1}$  the application of thermal paste will minimize thermal resistance on the interface.

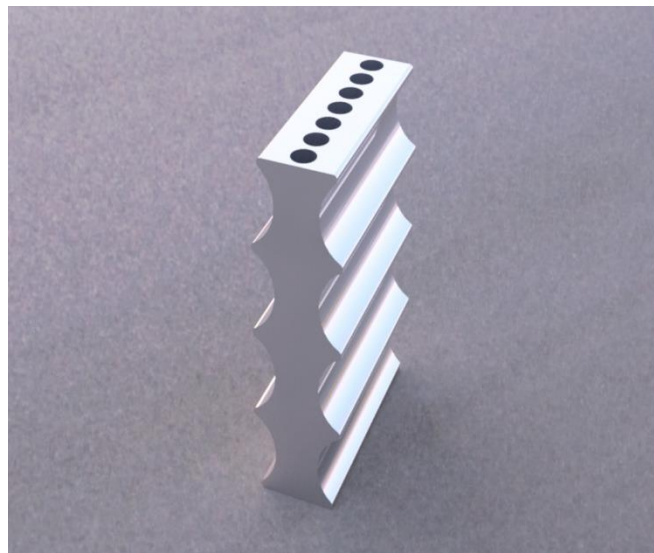


*Figure 33: Heat Sink*

### 8.2. Heat Pipes

Copper heat pipes with sintered wicks and nominal dimensions of 176 mm and 6 mm in length and diameter respectively are used for our cooling system. The heat pipes are expected to have an effective thermal conductivity of over 10000  $\text{Wm}^{-1}\text{K}^{-1}$ . The dimensions of the heat pipes were decided after considering their maximum heat transfer rate of 63 W per heat pipe and our maximum waste heat generation rate of 13 kW. If they

are loaded past their maximum heat transfer rate, they will not be able to perform at expected efficiency.

Since heat pipes use liquid-vapor phase change to transfer heat effectively, their efficiency is limited by physical factors. At relatively low temperatures of below 50 °C, the entrainment limit and capillary limit are dominant. These limits are controlled by heat pipe dimensions, such as length, diameter, wick thickness, pore radius, pore density, wick permeability, and properties of the liquid and vapor inside the heat pipe. Since we were unable to acquire all of the variables that were needed to perform a quantitative analysis, our decisions were based on the presumed experimental data provided by the sponsor and manufacturer, Novark Technologies.

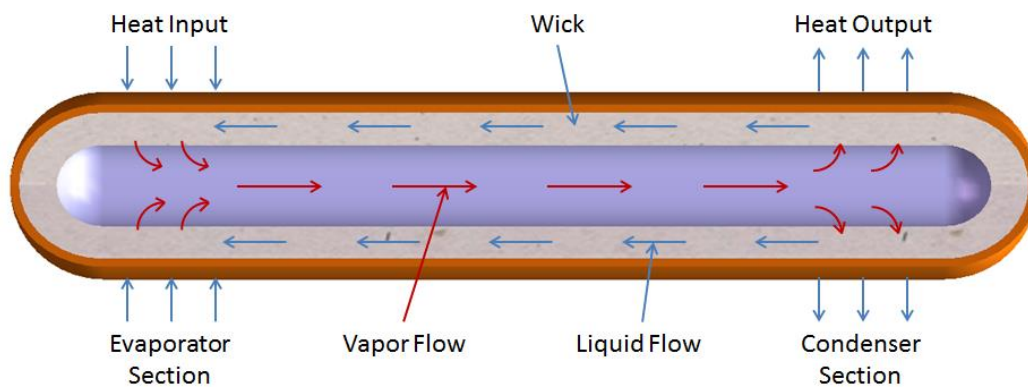
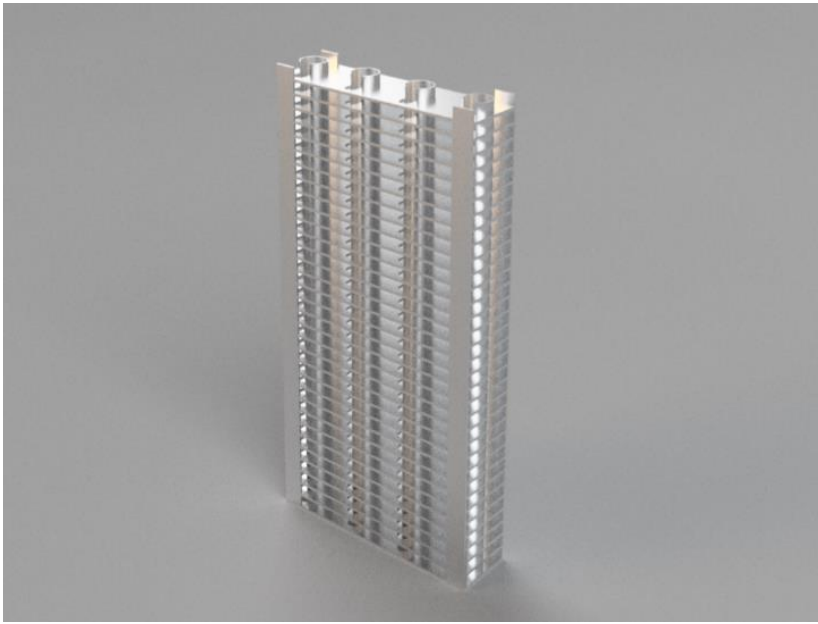


Figure 34: Heat Pipe

### 8.3. Fins

The fins will be stamped, by Novark Technologies, from 0.5 mm aluminum to the dimensions of 53.5 x 15 mm. These fins will be soldered onto the heat pipes. This will ensure that there will be a minimal amount of contact resistance in the system. The fin array was designed to reject 983 W of heat to the ambient air the car will be in and creates a 900 Pa pressure drop within the accumulator housing with the proper fin housing. This was figured by analytical calculations and simulations, however, so further tests will need to be conducted to ensure the fin array does not need to be modified. This design can be seen in Figure 35. The full assembly with the fins inside the heat sinks can be seen in Figure 36.



*Figure 35: Fin Design*

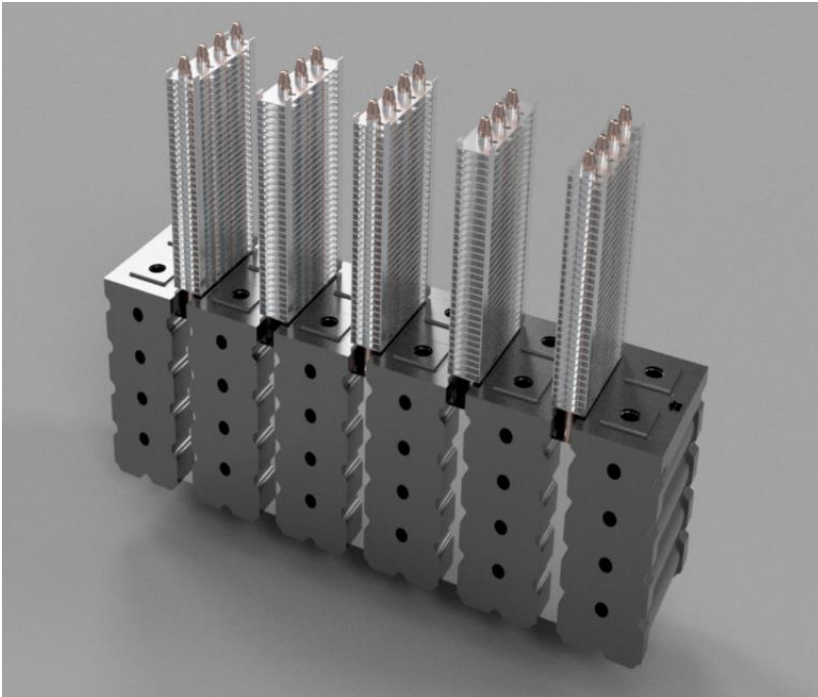


*Figure 36: Sample of Heat Sinks, Heat Pipes and Fins*

## 8.4. Fans

Based on the pressure drop and heat transfer requirements, we have decided to use the fan model 4118 N/2H8P, manufactured by EBM-PAPST. Figures 37 and 38 detail the technical specifications of the fan.



Type	4118 N/2H8P	
Nominal voltage	VDC	48
Nominal voltage range	VDC	36 .. 60
Speed (rpm)	min <sup>-1</sup>	11000
Power consumption	W	120
Min. ambient temperature	°C	-20
Max. ambient temperature	°C	75
Air flow	m <sup>3</sup> /h	570
Sound power level	B	8.9
Sound pressure level	dB(A)	78

Figure 37: Fan Specs

Technical description	
General description	Power consumption when wide open; these values may be considerably higher at the operating point.
Impeller material	Glass-fiber reinforced PA plastic
Weight	0.425 kg
Dimensions	119 x 119 x 38 mm
Housing material	Die-cast aluminum
Airflow direction	Intake over struts
Direction of rotation	Clockwise, viewed toward rotor
Storage	Ball bearing
Service life L10 at 40 °C	55000 h
Service life L10 at maximum temperature	22500 h
Cable	Leads AWG 20, sensor and control leads AWG 22, UL 1007, TR 64, stripped and tin-plated.
Motor protection	Protection against reverse polarity and blocked rotor.
Option	Other inputs and outputs. 36-72 VDC possible.

Figure 38: Fan Technical Description

The shaded area of Figure 39 indicates the operational zone of our fan. Although this fan is not able to provide enough pressure within its operational limits to overcome the expected pressure drop of 900 Pa, two fans in series will provide enough pressure while maintaining the flow rate. This argument is supported by Figure 40. During actual fan operations, we aim to maintain the fan performance between 180 and 225 CFM for the following reasons. Although the operational limits are set from 140 to 250 CFM, not all the values from this range meet our requirements. From 140 to 180 CFM, different airflow rate values are given for a same pressure drop. This implies potential fluctuation of airflow rate for that given pressure drop, which may result in fluctuation of accumulator temperature. From 225 and 250 CFM, the fan is unable to meet the pressure drop requirements even if two fans are used in series.

Therefore, 6 fans connected in series of 3x2 will be used to fulfill the pressure drop requirement while maintaining a stable air flow between 180 and 225 CFM. The exact flow rate shall be determined experimentally, after the accumulator housing dimensions are decided.

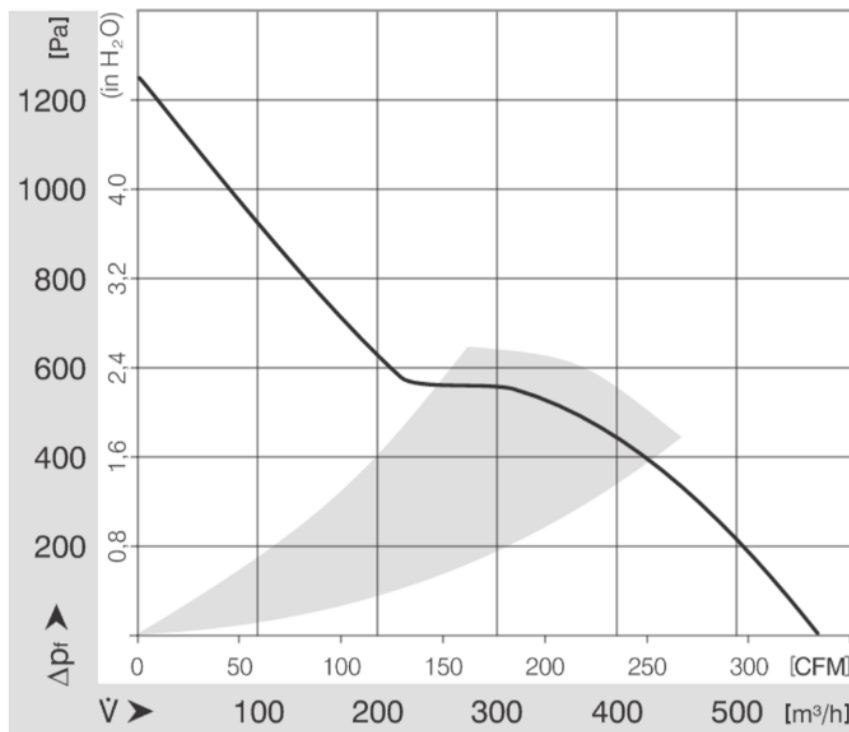


Figure 39: Fan Operation Curve

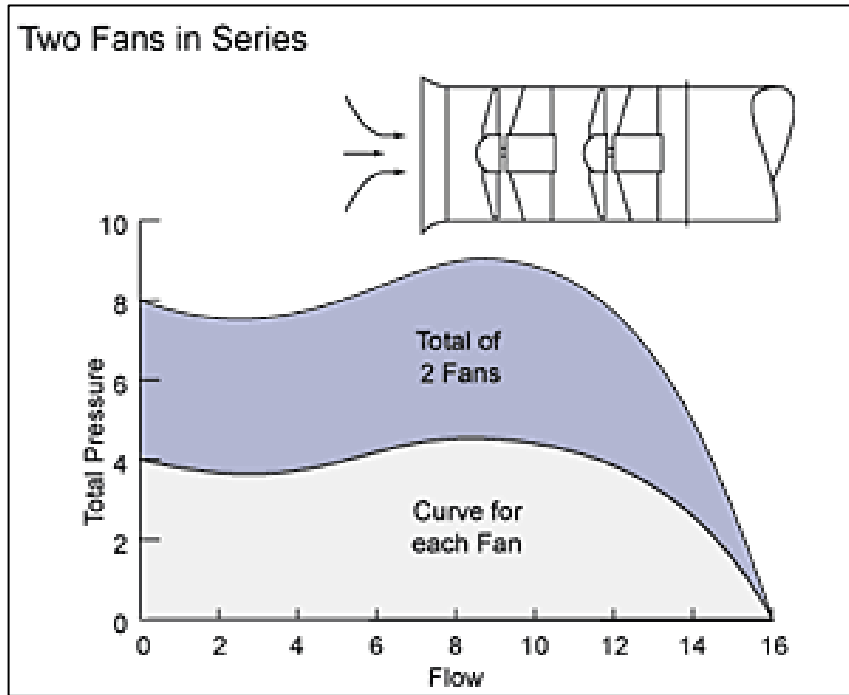


Figure 40: Typical Behavior of Two Fans in Series

### 8.5. Accumulator Case

Since three fans are going to be installed on each end of the accumulator which has five rows of fin arrays, a housing structure has been designed to maintain the air flow perpendicular to the fin arrays. Three 120 mm wide fans fit almost perfectly to the 360 mm wide accumulator. The width of each duct shall be decided experimentally to satisfy the pressure drop and flow rate requirements of our cooling system.

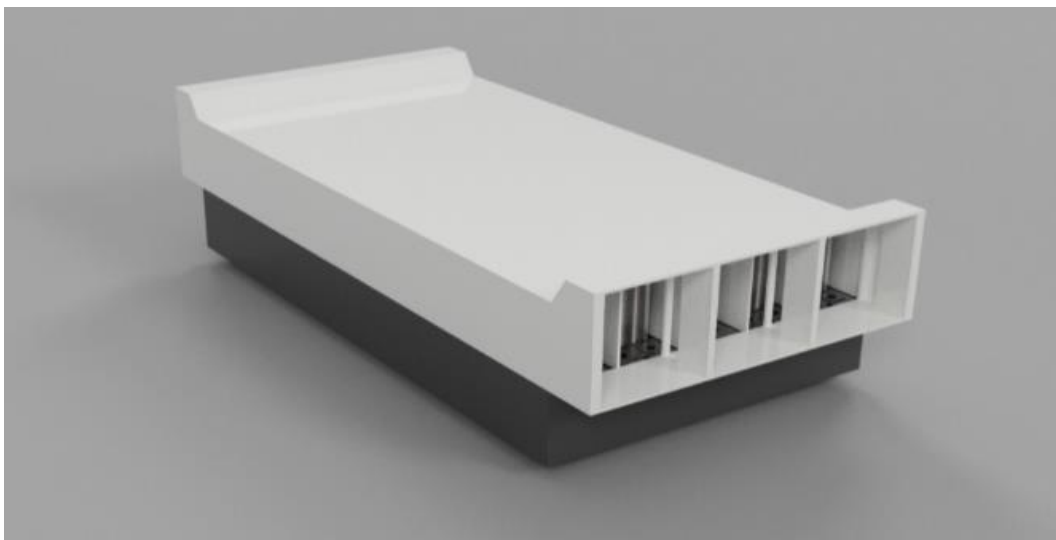
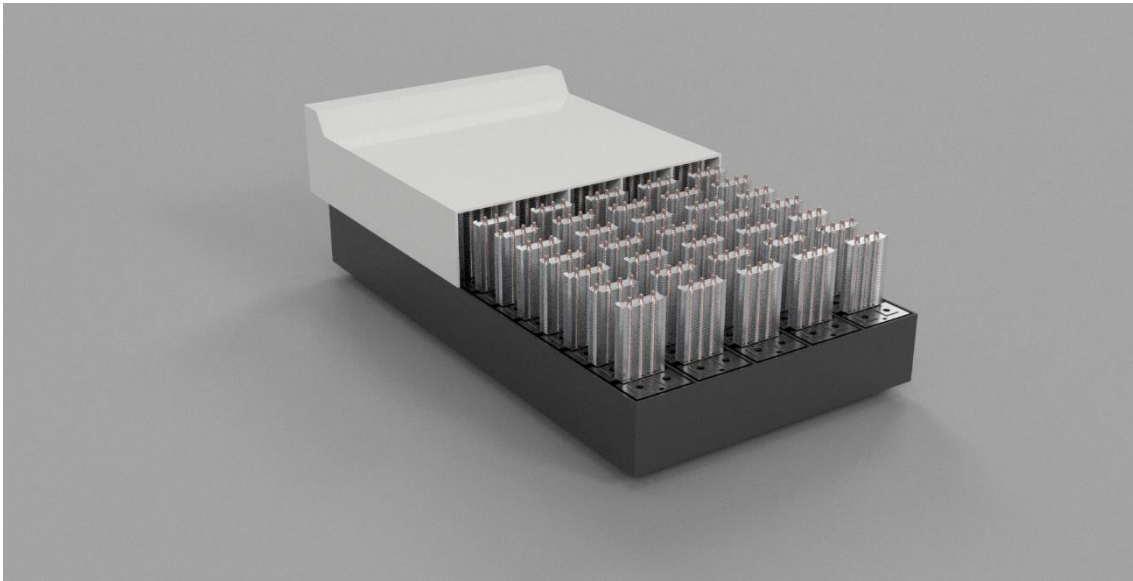


Figure 41: Final Design Configuration



*Figure 42: Final Design Half Cut*

## **8.6. Phase-Change Materials**

Only 3 or 4 out of the 7 holes on each aluminum heat sink will be used for heat pipe insertion. As a safety measure, we can insert phase-changing materials (PCM) inside the remaining empty holes. The specific type of PCM we are considering, A48 organic PCM solution manufactured by PCM Products Ltd has a melting temperature of 48 °C, and a latent heat of fusion of 230 J/g. This means if the accumulator happens to exceed the target operating temperature of 45 °C, the PCM will be able to absorb a large amount of heat when the temperature further exceed to 48 °C until the PCM completely melts after 7 seconds at maximum acceleration, thus acting as a last safety measure.



## 9. FUTURE EXPERIMENTS

We have proven that our cooling system is able to achieve a heat rejection rate higher than the average waste heat generation rate of the accumulator while maintaining a flow rate of 180 to 225 CFM and a pressure drop of 900 Pa from the combination of simulations, calculations, and experiments.

Once the prototype and additional battery modules arrive, IFE and future teams who work on this project can conduct a heat rejection experiment of the accumulator. Since the sensors used for this project are extremely difficult to implement inside the IFE vehicle, it is recommended this experiment to take place outside the vehicle. However, the experiment will use the motor and fans instead of power resistors and wind tunnels to replicate actual operational conditions as much as possible.

This experiment has two different aims. First, it will be possible to optimize fin housing dimensions and finalize the cooling system design by conducting a thorough experimentation and measurement of flow rate, temperature, and pressure at the inlet and outlet of the air path. After all the components of our cooling system are assembled together, repeating the same experiment will insure its performance.

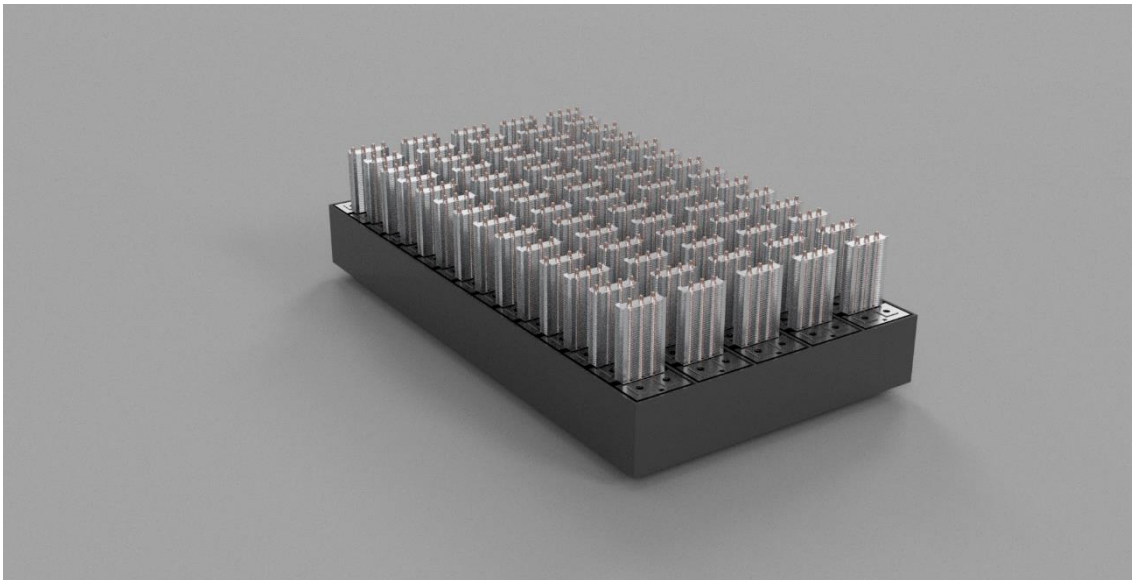


*Figure 43: Final Design no Case*



## 10. PROJECT DELIVERABLES AND BUDGET

The main project deliverables include the identification and quantification of heat sources and design of cooling system for the accumulator. Heat sources were modeled using electrical and chemical waste heat, based on the discharge experiments of battery modules. CAD drawing of the cooling system has been submitted to the sponsor to manufacture. Calculations of convective heat transfer from fins, FEA simulations for conduction through heat sinks and heat pipes, and CFD simulations for a full array of accumulator and the cooling system have been detailed in this report. Pressure drop experiments have also been conducted at the wind tunnel to confirm performance and to provide a standard for fan choice. This information will be handed over to IFE for further investigation.

A total of \$1384 was spent for this project. We have purchased two battery modules to conduct discharge experiments. We also plan to buy 6 fans for actual use on our cooling system. The rest of the expenses were spent on material for experimental purposes. Table below details our budget for the project.

<b>Item</b>	<b>Cost \$</b>
Power Resistor	48.60
12 Gauge Wire	5.24
Vertical Lever Actuator	35.18
Alligator Clip Sleeve	8.16
2-Pin Female Alligator Clip	6.98
Insulating Washer	2.80
Battery Terminal Connector	11.63
Battery Modules	232.12
3D Printing	3.15
Fans	780
<b>Total</b>	<b>1382.12</b>

*Table 8: Budget Spent*

As it can be seen, this budget does not include the cost of the final design, as it will be manufactured by Novark Technologies with no cost, so no budget was assigned to it. The rest of the battery modules will be purchased by IFE, so there are not expenses related to it as well.

## 11. CONCLUSIONS

In this project we aimed to identify and quantify the amount of heat we needed to reject, designed a cooling system for that waste heat, predicted its performance analytically, and placed the order for the prototype to be manufactured. Unfortunately, we were not able to fully evaluate the actual performance of our cooling system design. We did not have a precedent model of a cooling system and focused the majority of our time on researching other systems and our constraints before being able to begin the design. The prototypes and the battery modules that will be implemented into next year's design for the IFE vehicle have yet to arrive but have been ordered.

Major contributing factors towards our goals include the support from Novark Technologies Inc.; without this our project would not have been possible or within budget. The major costs of the prototype were graciously donated, these include materials and manufacturing. Secondary contributing factors include initiative to start work with no past reference or background to. We expect that our design will be of great help to Illini Formula Electric, and hope that future teams that work on this project will improve our design even more. Based off of the pressure drop analysis, we recommend pursuing a different accumulator configuration that would limit the flow length and eliminate the need for multiple fans.

An alternative approach could implement the use of the on-board water cooling system of the vehicle, however this would have to be in conjunction with the IFE water cooling team. The water would be received downstream and the water pump would have to be redesigned to handle a greater load.

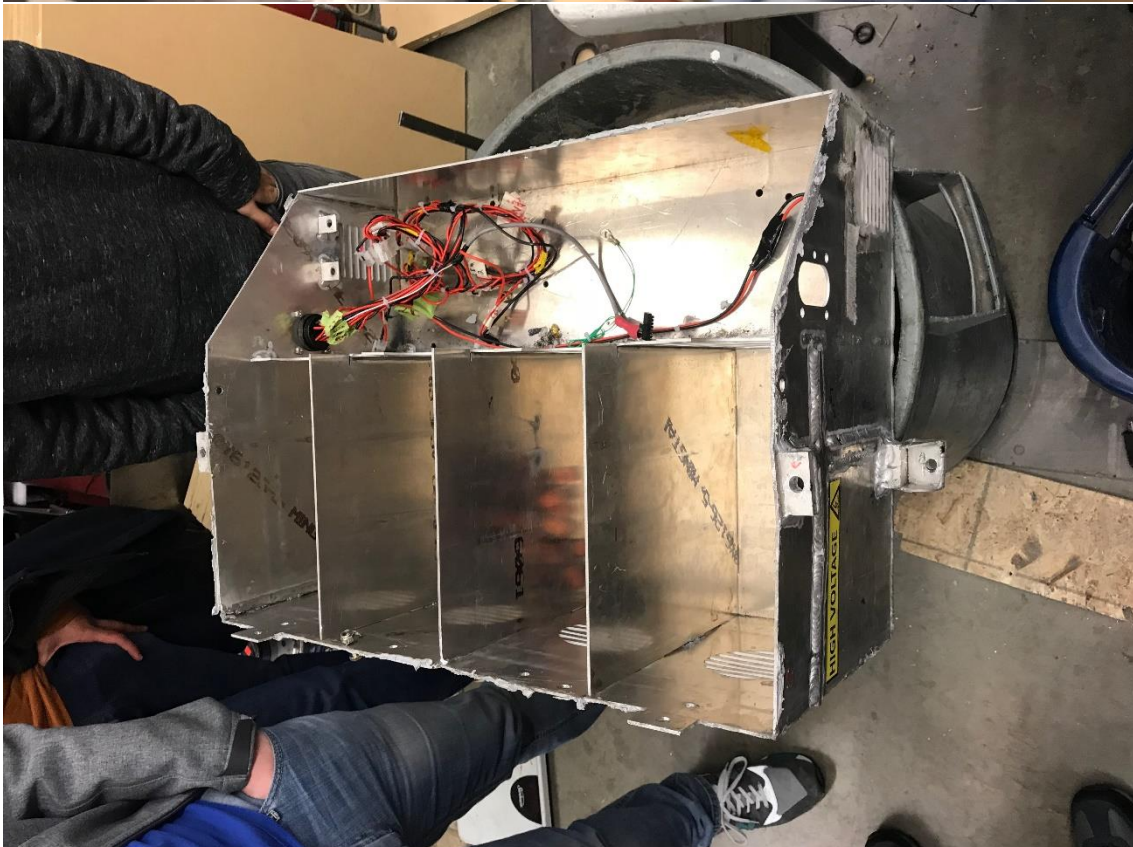


## 12. REFERENCES

- [1] Wikipedia contributors. Formula SAE. Wikipedia, The Free Encyclopedia [https://en.wikipedia.org/wiki/Formula SAE](https://en.wikipedia.org/wiki/Formula_SAE) 31
- [2] SAE International. 2017-18 Formula SAE Rules PDF, 2018.
- [3] Eneragus Power Solutions Ltd.  
<https://www.eneragusps.com/page/homepage>
- [4] Dong Hyup Jeon, Seung Man Baek. Thermal Modeling of Cylindrical Lithium Ion Battery during Discharge Cycle Energy Conversion and Management, Volume 52, Issues 8-9, Pages 2973-2981, 2011.
- [5] A. Nir. Heat Transfer and Friction Factor Correlations for Crossflow over Staggered Finned Tube Banks Heat Transfer Engineering, 12:1, 43-58, 1991.
- [6] Samsung SDI. Specification of Product. PDF, 2014.
- [7] Best 18650 Battery at 0.2 Ohm or 16-21A Pulsed Loads. <https://liionwholesale.com/blogs/reviews-and-test-results/49049156-best-18650-battery-at-0-2-ohm-or-16-21a-pulsed-loads>
- [8] Maleki et al. Thermal Properties of Lithium-Ion Battery and Components J. Electrochem. Soc. volume 146, issue 3, 947-954m, 1999.
- [9] Eneragus Power Solutions Ltd. Li-ion building block Li8P25RT.. PDF, 2017.
- [10] F. P. Incropera, D.P. Dewitt, T.L. Bergman, A.S. Lavine. Fundamentals of Heat and Mass Transfer. Wiley, 2011.
- [11] Novark Technologies. <https://www.novarktechnologies.com/>
- [12] PCM Products. <http://www.pcmproducts.net/files/PCM%20Summary%202013-A.pdf>
- [13] EBM-PAPST. <http://www.ebmpapst.us/en/>
- [14] Wang, Chi-Chuan, et al. Heat Transfer and Friction Characteristics of Plain Fin-and-Tube Heat Exchangers, Part II: Correlation. International Journal of Heat and Mass Transfer, vol. 43, no. 15, 2000, pp. 2693-2700., doi:10.1016/s0017-9310(99)00333-6.

[15] Transmisión de Calor, Comillas ICAI  
[https://sifo.comillas.edu/pluginfile.php/979148/mod\\_resource/content/0/07%20Aletas.p  
df](https://sifo.comillas.edu/pluginfile.php/979148/mod_resource/content/0/07%20Aletas.pdf)

### 13. APPENDIX A: OLD ACCUMULATOR

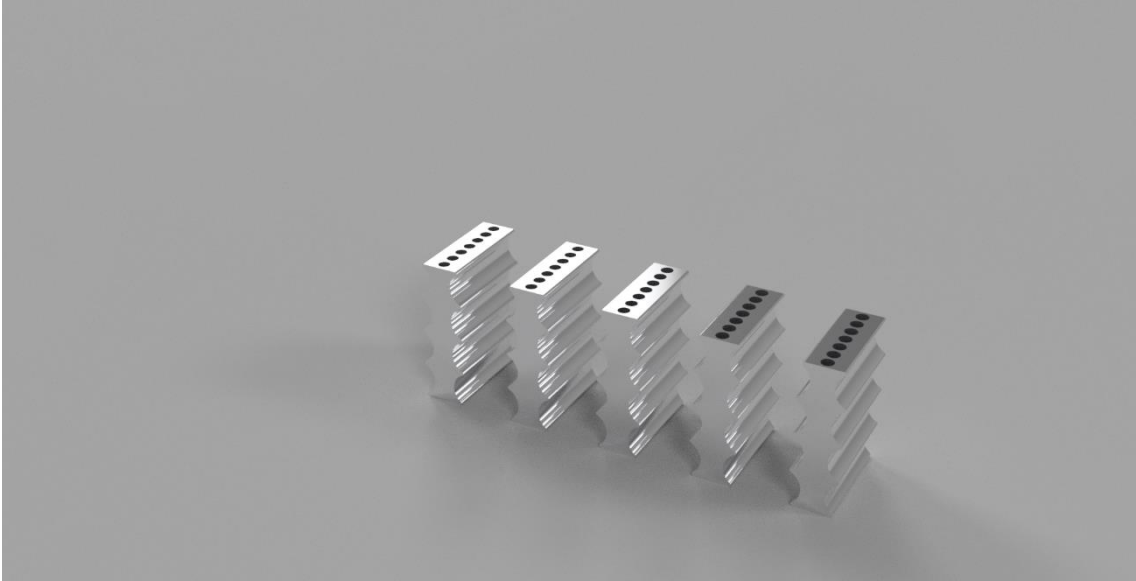
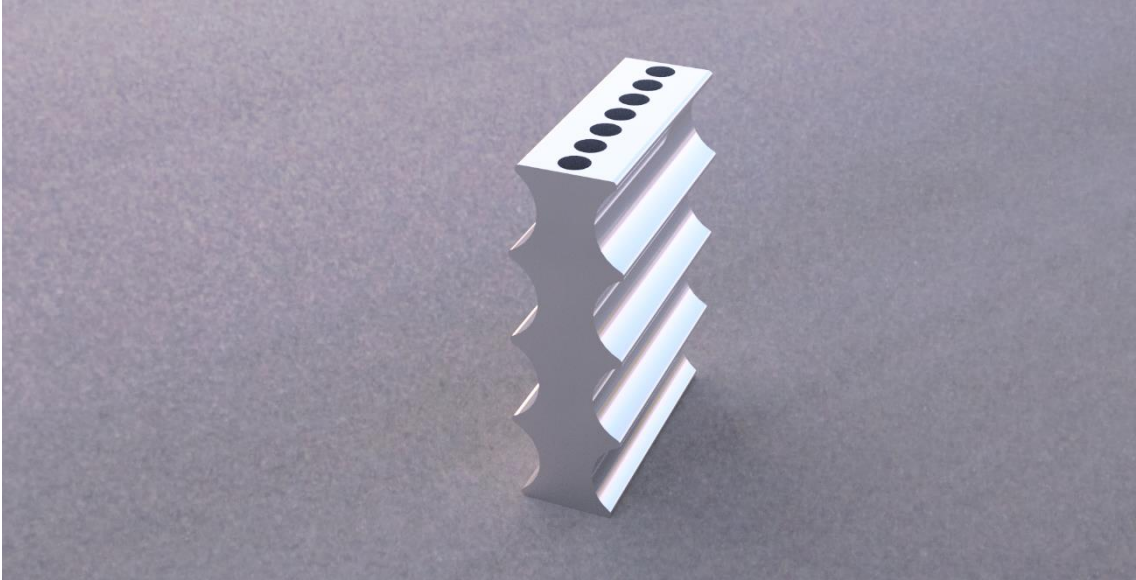
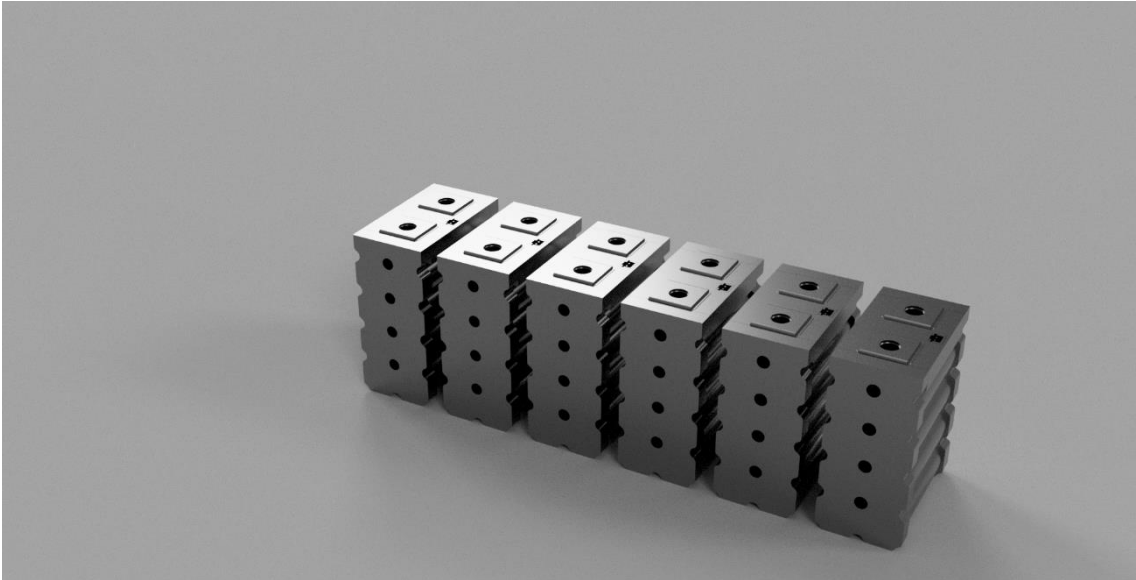


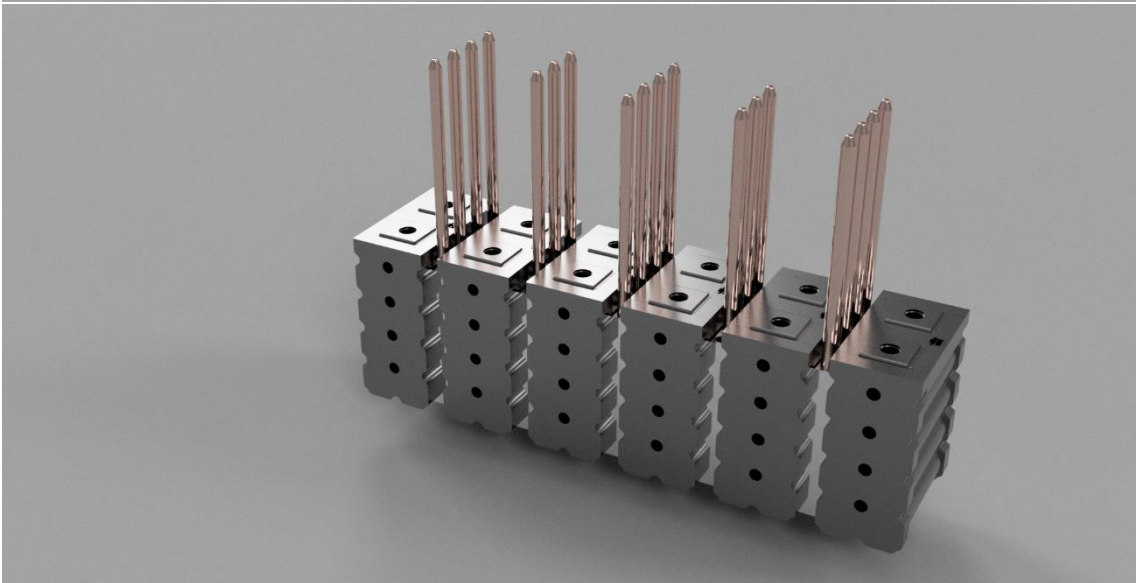
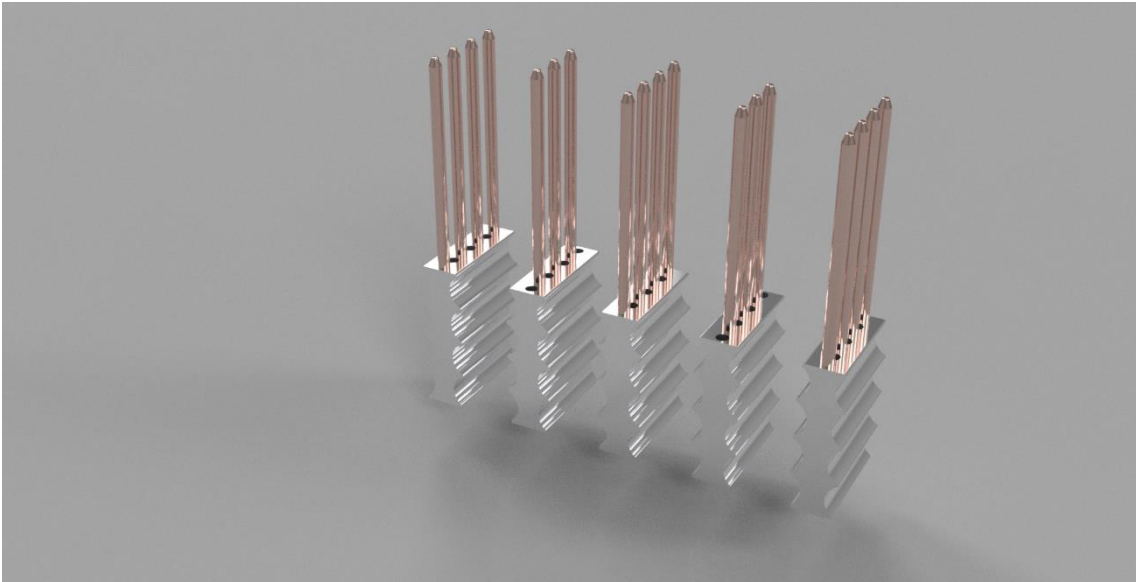
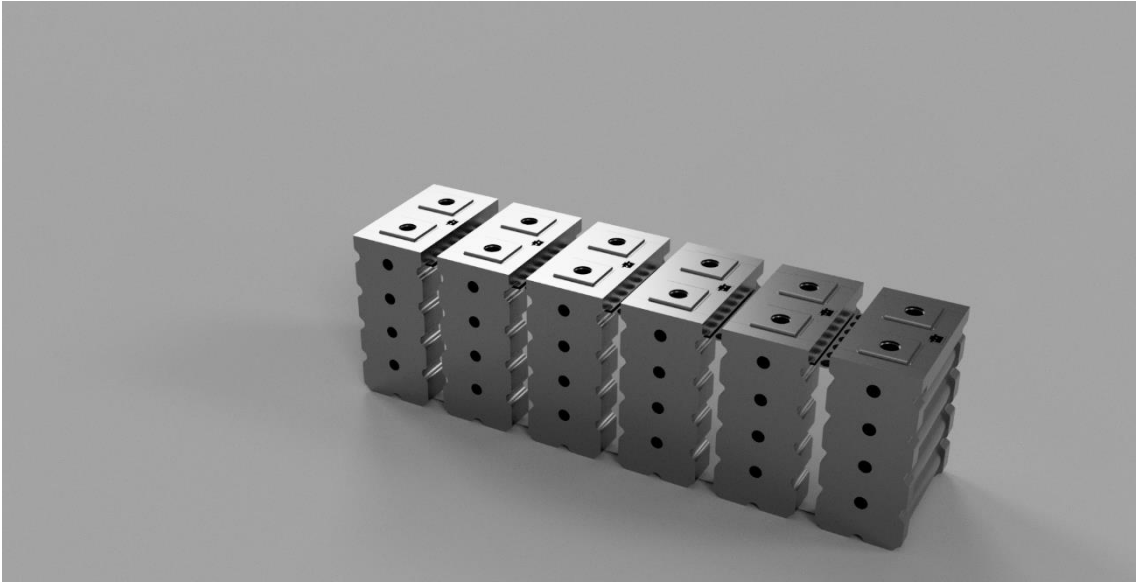


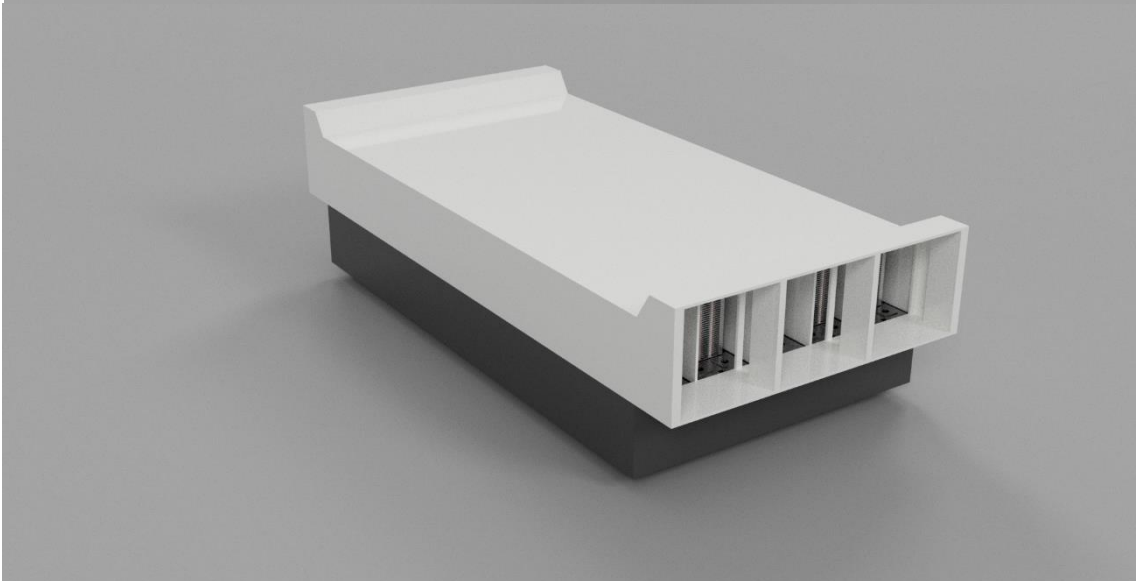
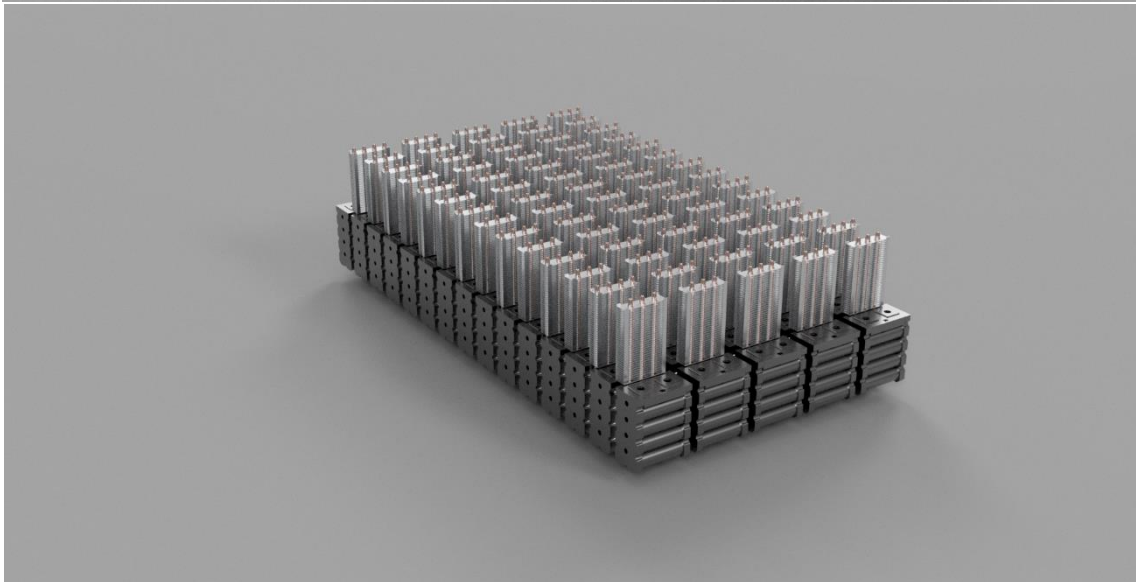
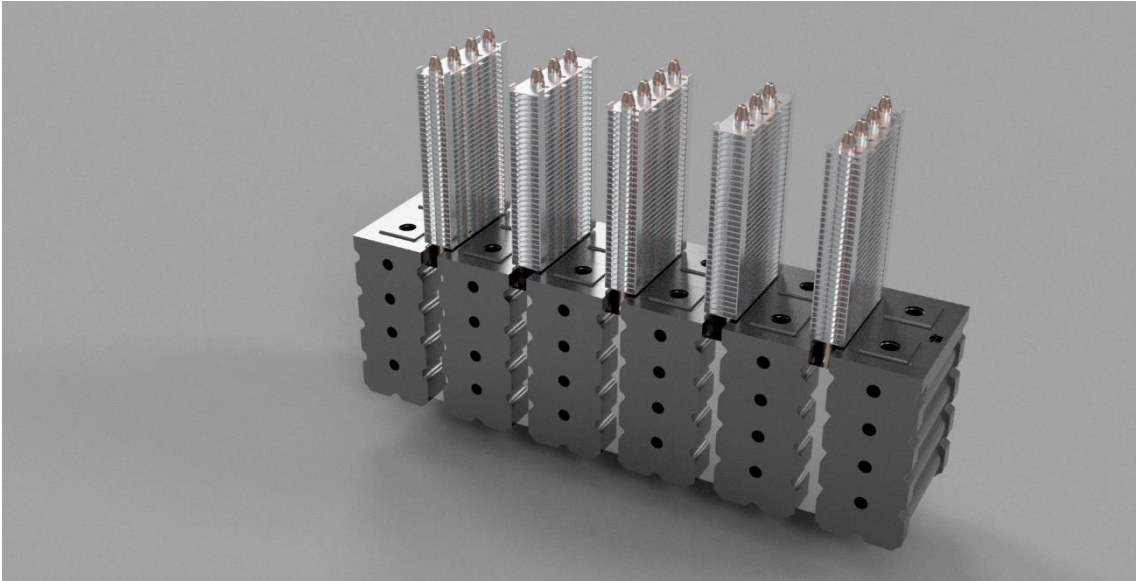


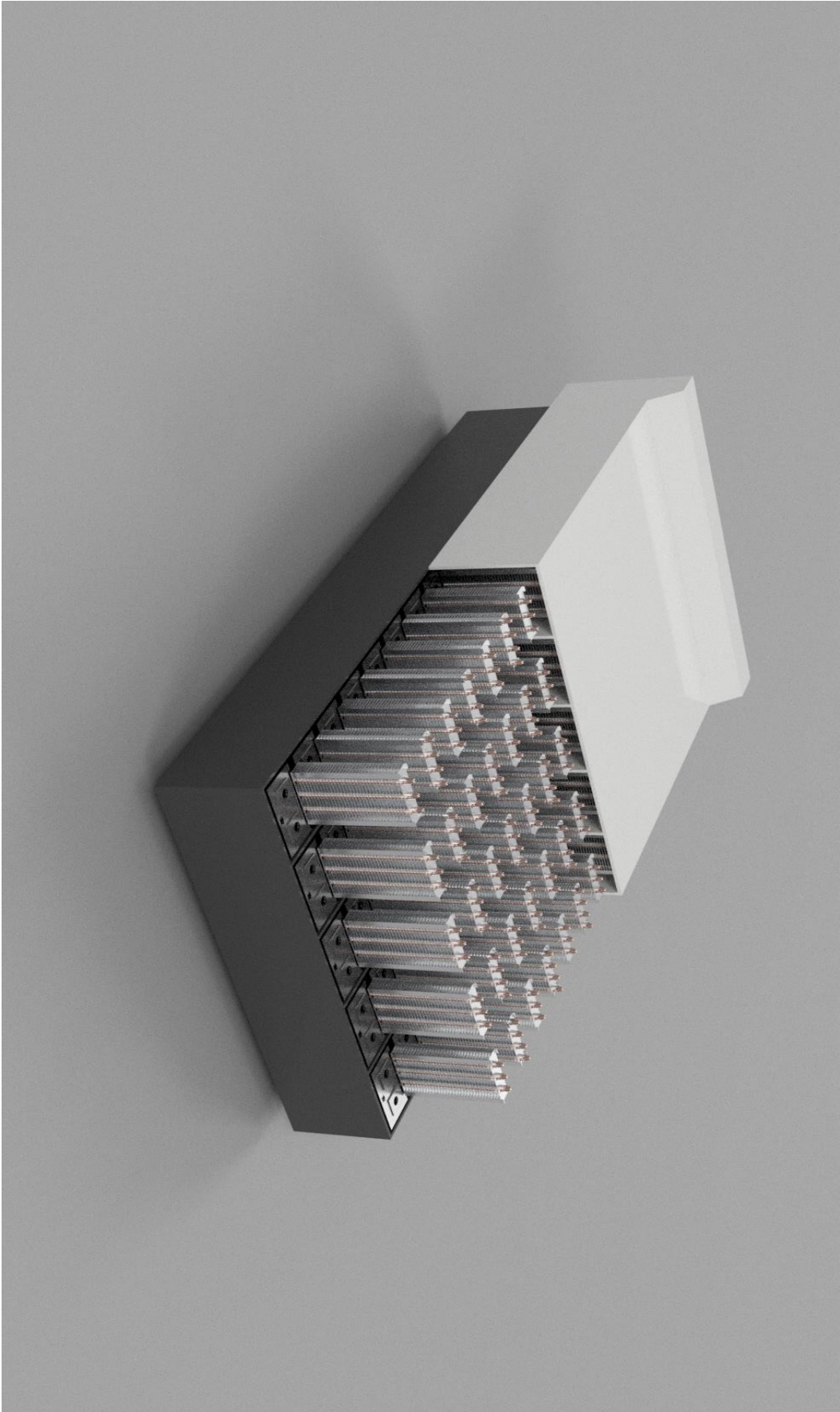


**14. APPENDIX B: CAD DESIGN**







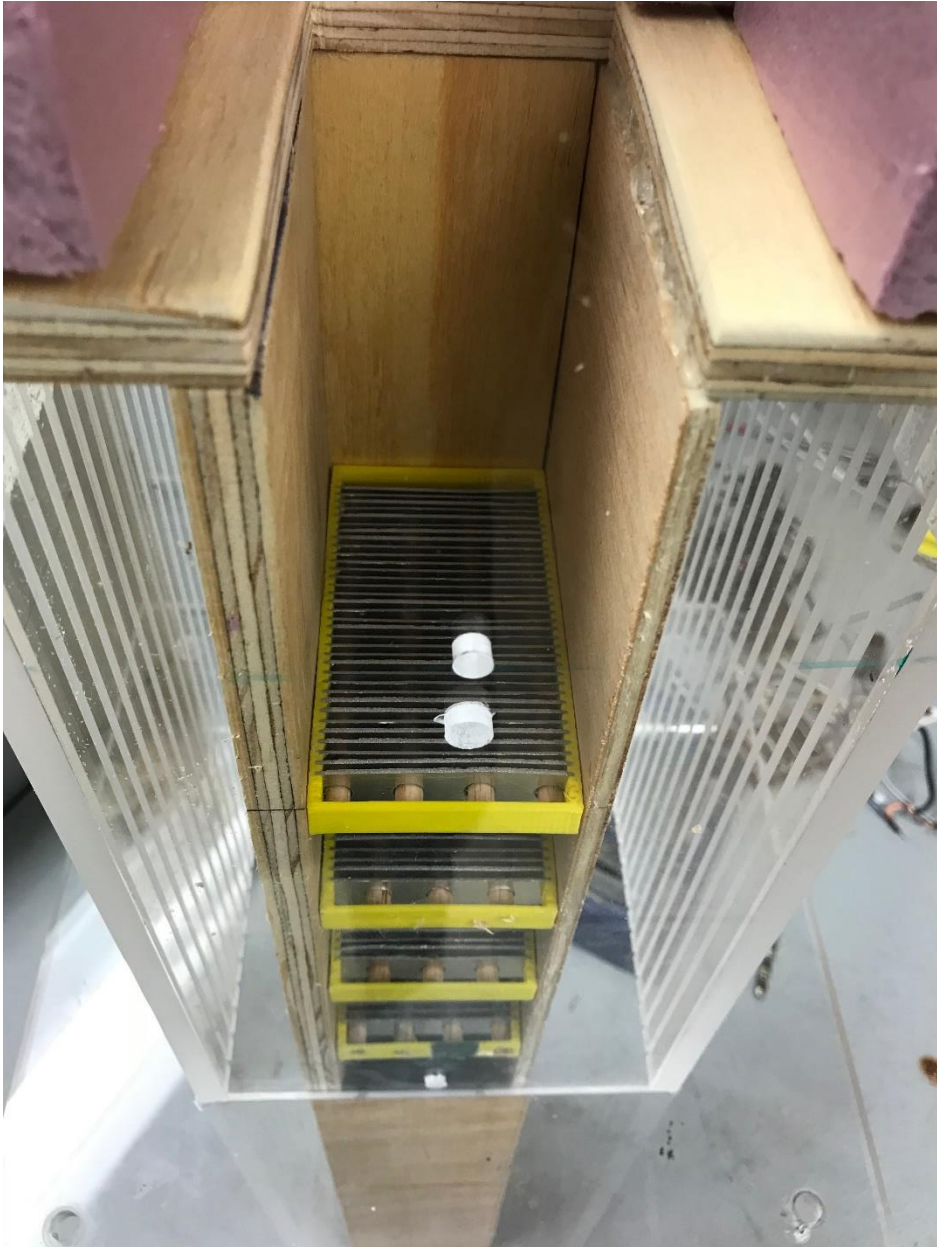


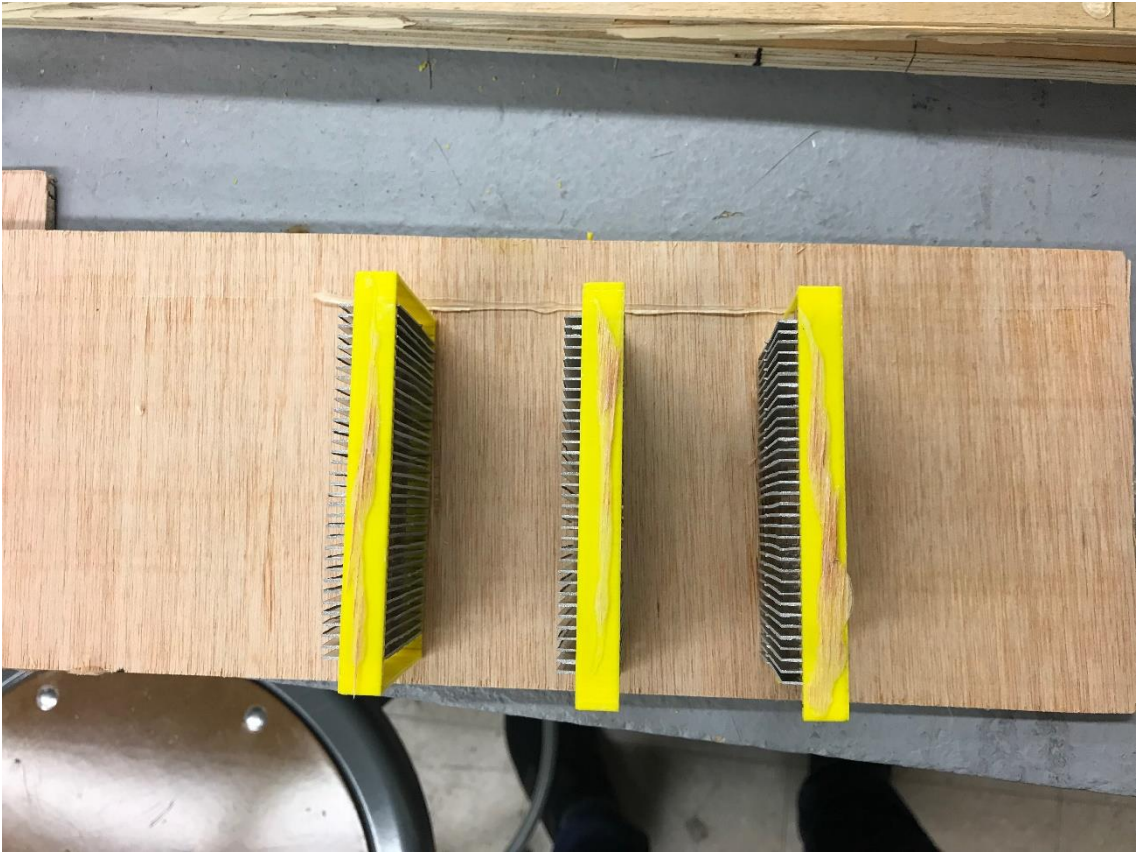
## 15. APPENDIX C: WIND TUNNEL SETUP







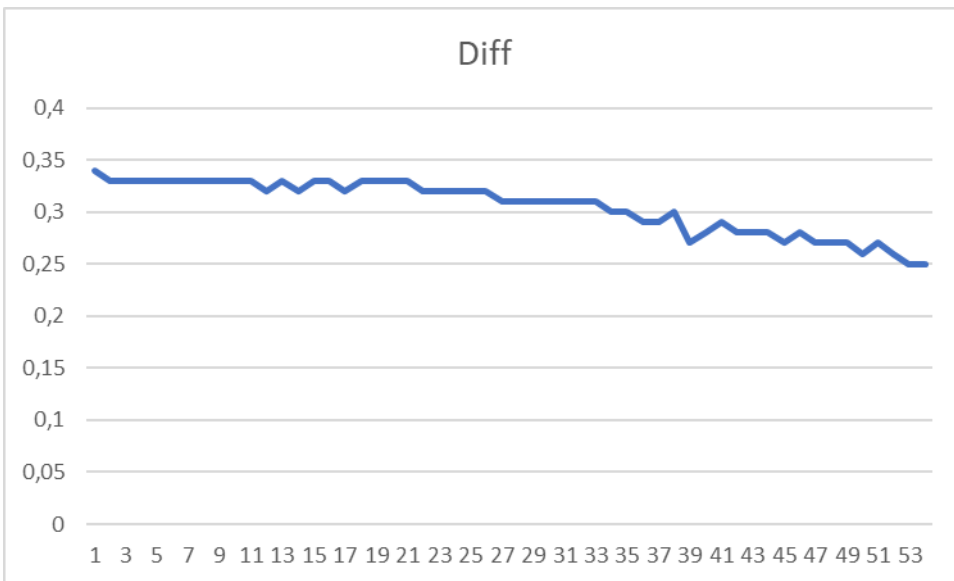
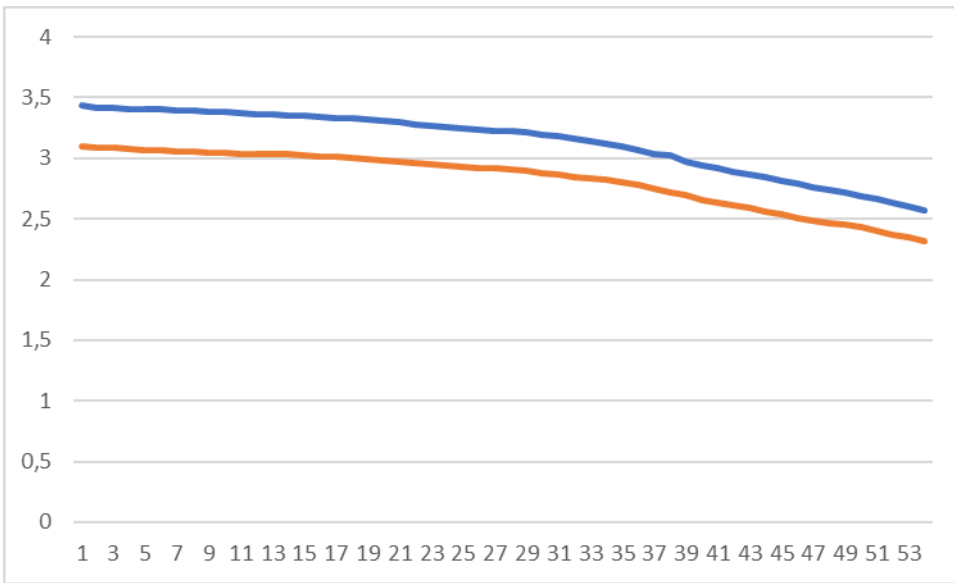


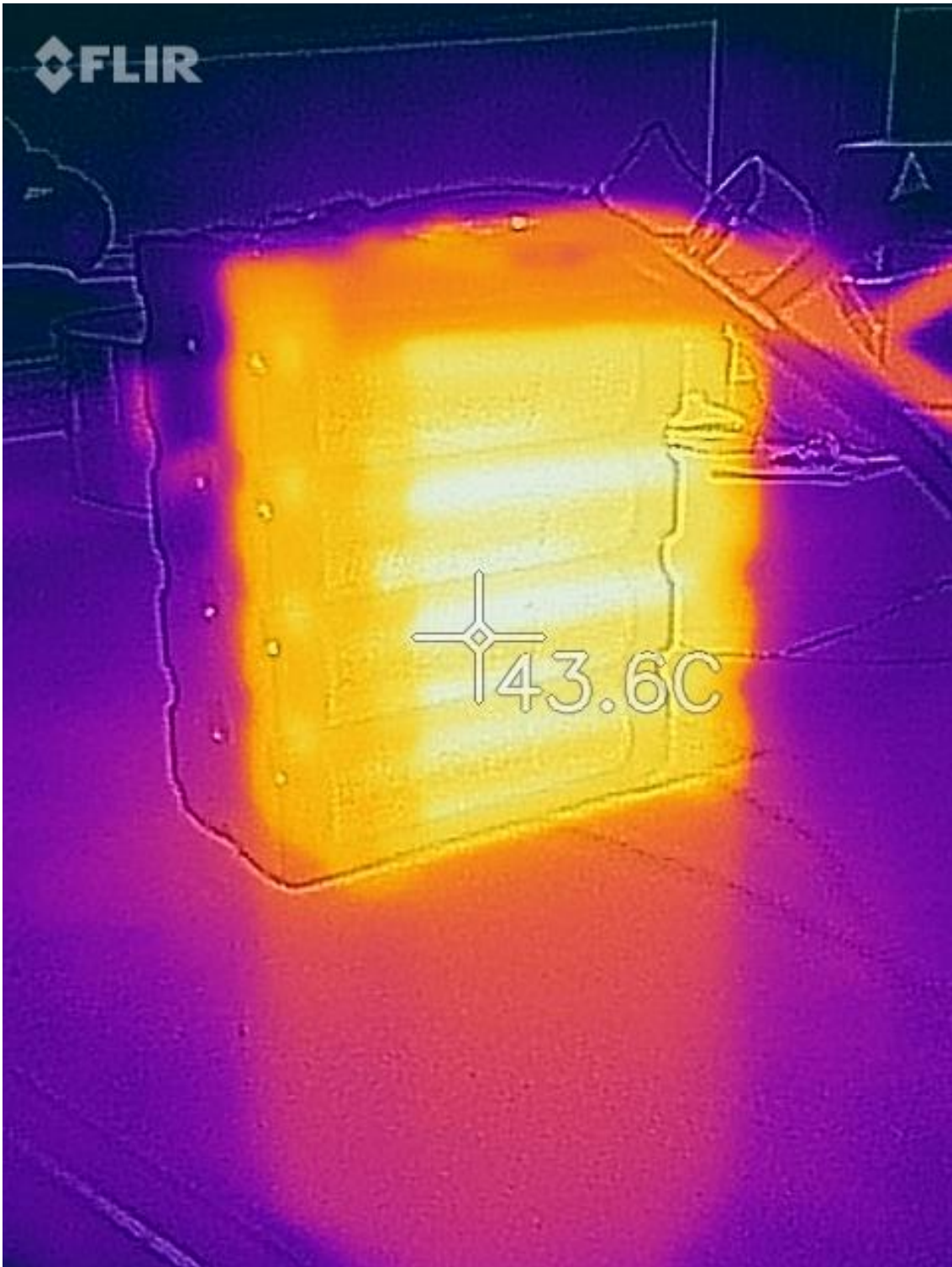


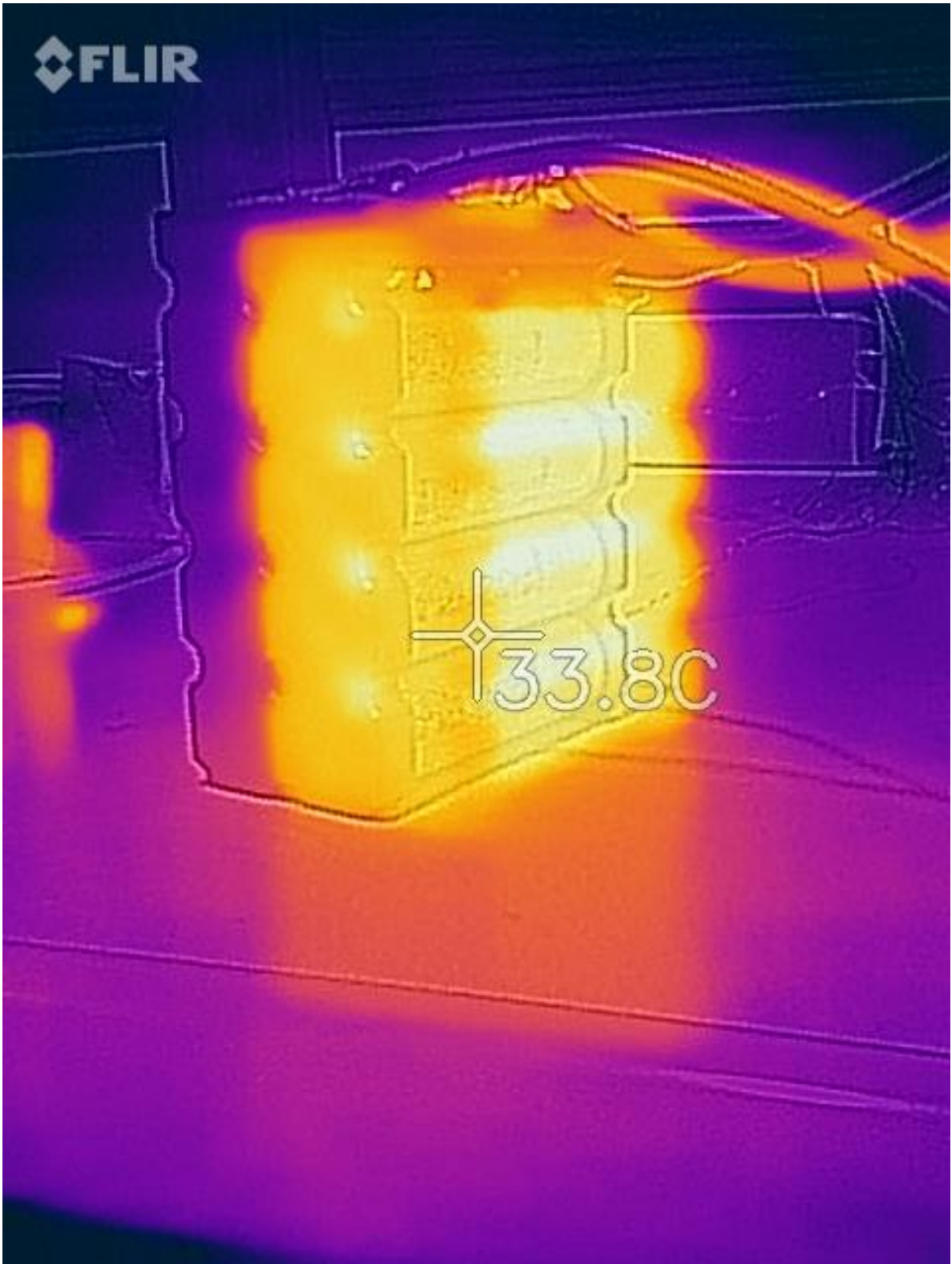


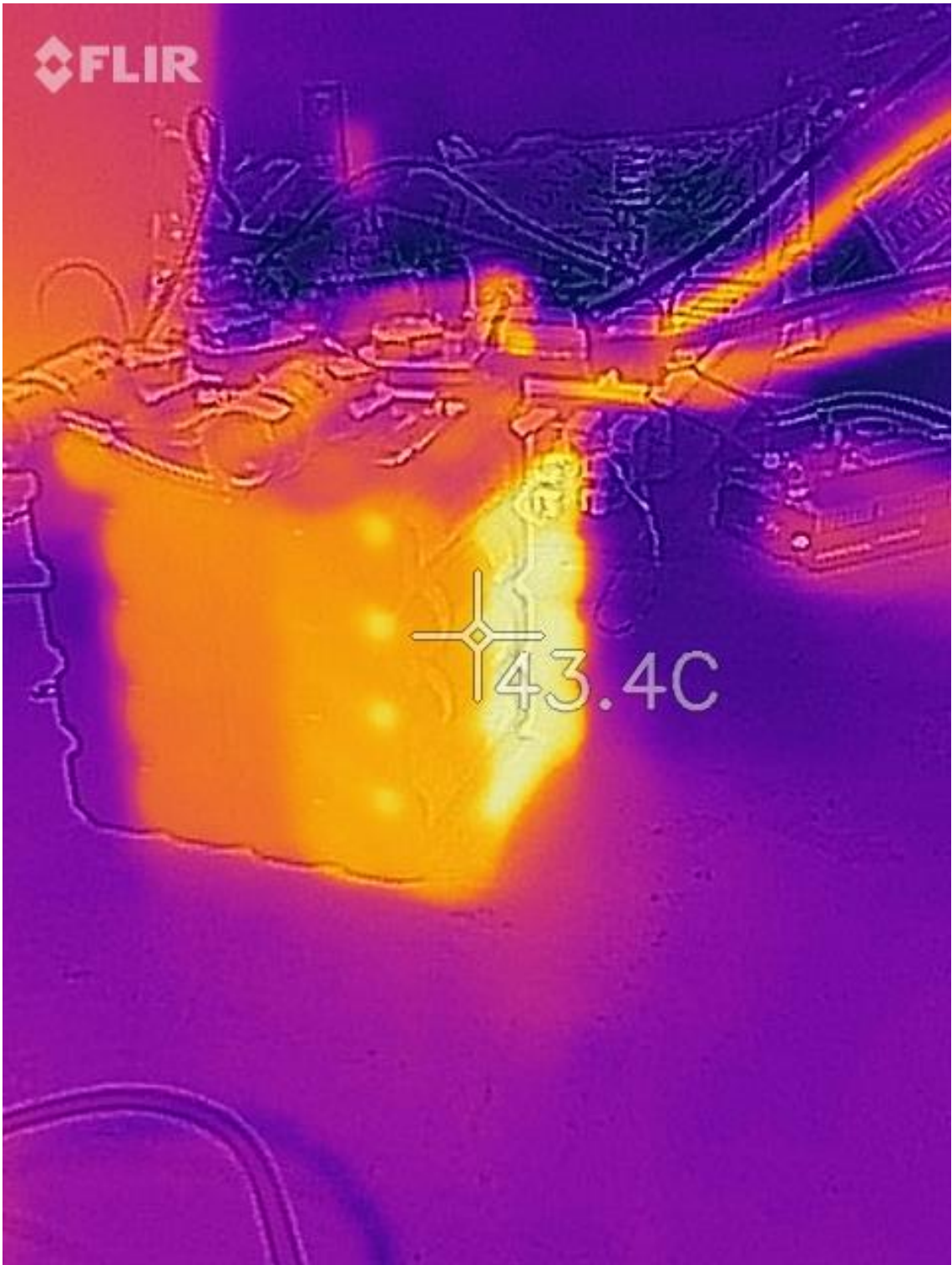
## 16. APPENDIX D: VOLTAGE EXPERIMENT

Multimeter	Arduino		Diff
3,1	3,44		0,34
3,09	3,42		0,33
3,09	3,42		0,33
3,08	3,41		0,33
3,07	3,4		0,33
3,07	3,4		0,33
3,06	3,39		0,33
3,06	3,39		0,33
3,05	3,38		0,33
3,05	3,38		0,33
3,04	3,37		0,33
3,04	3,36		0,32
3,03	3,36		0,33
3,03	3,35		0,32
3,02	3,35		0,33
3,01	3,34		0,33
3,01	3,33		0,32
3	3,33		0,33
2,99	3,32		0,33
2,98	3,31		0,33
2,97	3,3		0,33
2,96	3,28		0,32
2,95	3,27		0,32
2,94	3,26		0,32
2,93	3,25		0,32
2,92	3,24		0,32
2,92	3,23		0,31
2,91	3,22		0,31
2,9	3,21		0,31
2,88	3,19		0,31
2,87	3,18		0,31
2,85	3,16		0,31
2,83	3,14		0,31
2,82	3,12		0,3
2,8	3,1		0,3
2,78	3,07		0,29
2,75	3,04		0,29
2,72	3,02		0,3
2,7	2,97		0,27
2,66	2,94		0,28
2,63	2,92		0,29
2,61	2,89		0,28
2,59	2,87		0,28
2,56	2,84		0,28
2,54	2,81		0,27
2,51	2,79		0,28
2,49	2,76		0,27
2,47	2,74		0,27
2,45	2,72		0,27
2,43	2,69		0,26
2,4	2,67		0,27
2,37	2,63		0,26
2,35	2,6		0,25
2,32	2,57		0,25











## 17. APPENDIX E: FIN ANALYSIS MATLAB CODE

```
syms Q To
%For properties assume Tavg = (40+33)/2 = 36.5

T_inlet = 33; % Degrees Celcius into fin array
cp = 1007; % for T_avg_air
V_air = 5; % air speed in m/s
rho_air = 1.1378; % density of air at avg temp in kg/m3
width_row = 700e-3; % width of one row of battery m
height_frontal = (200e-3 - 80e-3); % height of fin array needed
to obtain perscribed dT
eq1 = Q == rho_air*V_air*cp*width_row*height_frontal*(To-
T_inlet);

D_fin = .01675; % Fin Diameter
d_tube = .006; % Tube Diamter

finThickness = .2e-3; % .5mm fin thickness
finSpacing = 1e-3; % 2 mm fin spacing
t=finThickness;
AreaFinTopBottom = 2*pi*((D_fin/2)^2-(d_tube/2)^2);
AreaFinSide = pi*D_fin*finThickness;
AreaSpacing = pi*d_tube*finSpacing;
A_l =
(AreaFinTopBottom+AreaFinSide+AreaSpacing)/(finSpacing+finThickn
ess); % Area of heat transfer per unit length finned tube (one
tube)
A_tot = A_l*3*14; % Area total for all 14*3 tubes of heat
transfer

A_R = AreaSpacing/(finSpacing+finThickness)
A_R_tot = A_R*14*3; % Area of tube surface for all 14*3 tubes

A_fin =
(AreaFinTopBottom+AreaFinSide)/(finSpacing+finThickness); %
Area of fin per unit length
A_fin_tot = A_fin*14*3; % Area of fin per unit length for all
tubes

k_air = 27.1e-3; %thermal conductiveity of air at Tavg
Pr = 0.7263; % prandtl number at Tavg
mu = 1.76e-5; %kinematic viscostiy of air at Tavg

L_char = d_tube*A_tot/A_R_tot
Re = V_air*(L_char)/mu;

X_l = .017; % Transverse pitch
X_t = .0476; % Longitudinal picthsposp

h_fin = D_fin-d_tube;

Nu = .1306*Re.75*Pr(1/3)*(A_tot/A_R_tot)(-.375)*((X_t-
d_tube)/(2*h_fin))(.21)*(X_l/X_t)(.4)
h_conv = Nu*k_air/L_char;

% Fin efficiency
hfin = D_fin-d_tube;
```

```

k_al = 180; % k of aluminum = 180 W/mK
phifin = 1+0.35*log(1+hfin/(d_tube/2));
mfin = sqrt(2*h_conv/k_al/finThickness);
finEff = tanh(mfin*hfin*phifin)/(mfin*hfin*phifin);
overEff = 1-(A_fin_tot/A_tot)*(1-finEff);

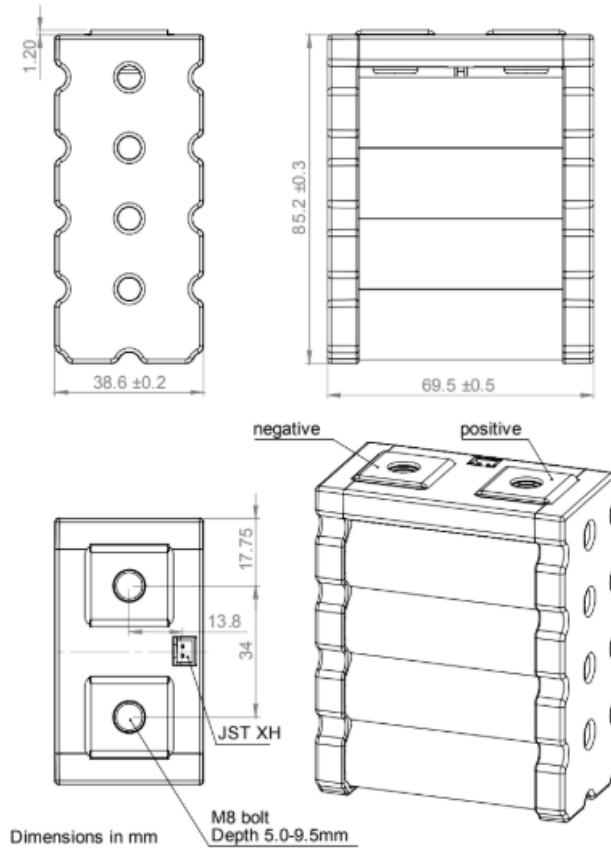
eq2 = Q == h_conv*A_tot*overEff*(Tb-To);

[Q To] = solve([eq1 eq2],[Q To])

```

# 18. APPENDIX F: BATTERY DATA SHEET

## MECHANICAL DATA



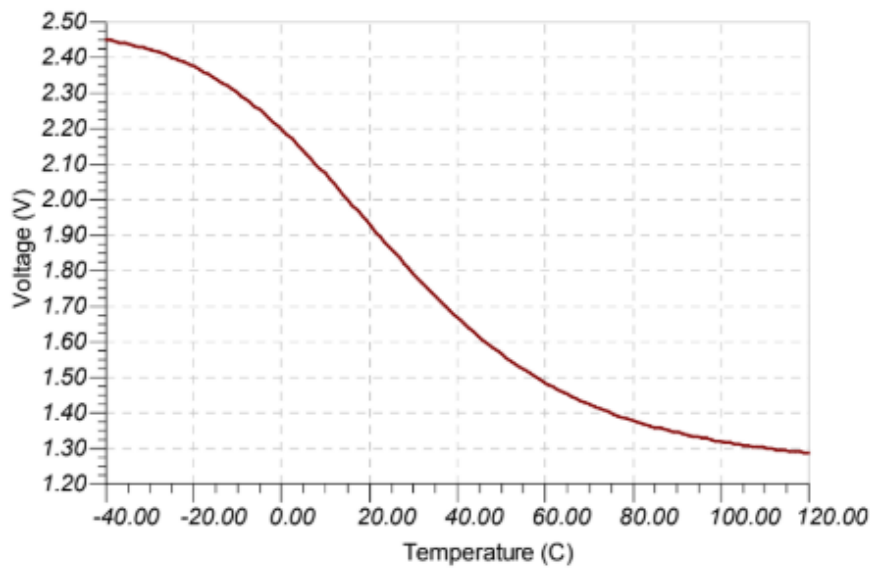
A simplified 3D STP model is available upon request.

### Notes:

1. Inner M8 nut is stainless steel
2. Tightening torque: 10 Nm
3. Self-locking washers recommended
4. Modules should be mounted in a firm enclosure to avoid mechanical damage.
5. Modules should be protected from direct water ingress.
6. Temperature sensor connector: JST XH series.

Table 2. Voltage-to-temperature conversion values

Temp, °C	-40	-35	-30	-25	-20	-15	-10	-5	0	5	10	15	20	25	30	35	40
V <sub>out</sub> , V	2.44	2.42	2.40	2.38	2.35	2.32	2.27	2.23	2.17	2.11	2.05	1.99	1.92	1.86	1.80	1.74	1.68
Temp, °C	45	50	55	60	65	70	75	80	85	90	95	100	105	110	115	120	
V <sub>out</sub> , V	1.63	1.59	1.55	1.51	1.48	1.45	1.43	1.40	1.38	1.37	1.35	1.34	1.33	1.32	1.31	1.30	



Parameter	Comment	Min.	Typ.	Max.	Unit
Battery voltage	Allowed range	2.50	3.60	4.20	V
Battery capacity	20A discharge to 2.5 V	19.5	20.4	-	Ah
	20A discharge to 2.5 V	70.2	73.4	-	Wh
	200A discharge to 2.5 V	18.5	19.5	-	Ah
Fast charge current	Forced air cooling	-	-	40	A
	No cooling, in a pack	-	-	30	A
	10 sec. pulse, 50% SOC	-	-	240	A
Discharge current	Forced air cooling	-	-	240	A
	No cooling, in a pack	-	-	120	A
	10 sec. pulse, fuse limited	-	-	360	A
Initial internal impedance	1kHz after rated charge	-	2.7	3.0	mΩ
Internal fuse rating	Holding current	-	-	360	A
Working temperature	Discharge	-20	25	60	°C
	Charge	0	25	45	°C
Dimensions	±0.5 mm	-	39×69.5×87	-	mm
Weight	Without fasteners	-	0.427	0.429	kg

## DISCHARGE CHARACTERISTICS

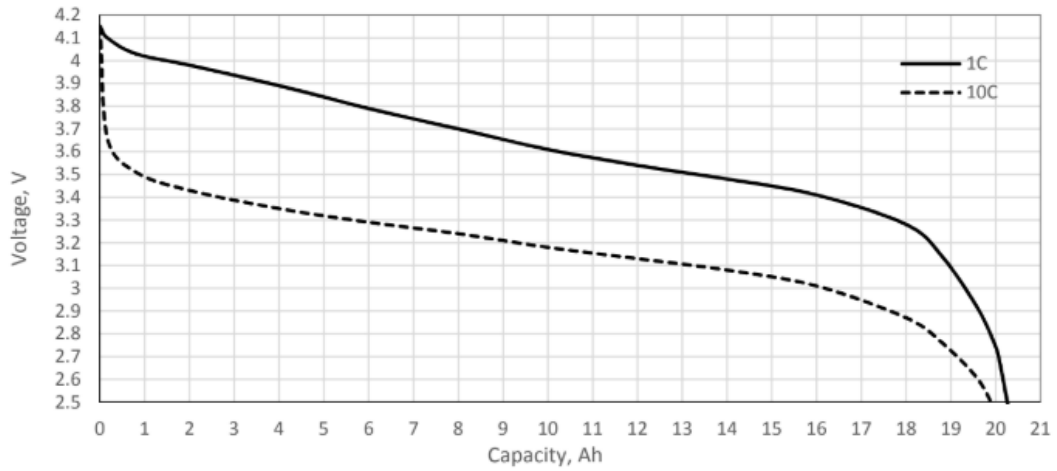


Figure 1. A typical discharge slope at 1.0C and 10C rate.

